Research Square

Preprints are preliminary reports that have not undergone peer review.
They should not be considered conclusive, used to inform clinical practice,
or referenced by the media as validated information.

Metal homeostasis and SirR regulation during denitrification in Haloferax mediterranei.

Jose María Miralles-Robledillo
University of Alicante
Alexandra Gabriela Simica
University of Alicante
Serena Rinaldo
Sapienza University of Rome
Rosa María Martínez-Espinosa
University of Alicante
Carmen Pire
carmen.pire@ua.es

University of Alicante

Research Article

Keywords: metal homeostasis, denitrification, haloarchaea, DtxR, SirR, iron uptake

Posted Date: November 4th, 2026

DOI: https://doi.org/10.21203/rs.3.rs-11207107/v1

License: This work is licensed under a Creative Commons Attribution 4.0 International License.
Read Full License

Additional Declarations: No competing interests reported.

Abstract

Haloferax mediterranei is a haloarchaeon capable of complete denitrification, reducing nitrate to dinitrogen. While this enzymatic pathway is known, the regulatory mechanisms coordinating metal homeostasis during this process remain poorly understood. Previous transcriptomic analyses revealed increased expression of the gene encoding SirR (E6P09_18060), a DtxR-family transcriptional repressor, during the early stages of denitrification under oxygen-limited conditions. In this study, we investigated the functional role of SirR through the characterization of gene deletion and overexpression strains. Cell growth and intracellular metal concentrations (Fe, Mn, Zn, Cu, and Mo) were analysed using optical density measurements and ICP-MS. The results showed substantial metal accumulation in early growth stages, with higher accumulation in the overexpression strain under various conditions. qRT-PCR analysis of two genes (E6P09_00145 and E6P09_02480) encoding iron transporters indicated that SirR could regulate E6P09_00145, which encodes a putative iron-binding protein. This regulation is significantly modulated by the interplay between iron and oxygen availability. Furthermore, bioinformatic analysis of iron-uptake gene promoters identified a conserved regulatory motif, and gel filtration chromatography of the purified protein confirmed that SirR functions as a homodimer. These findings establish direct regulatory links among SirR, metal homeostasis, and oxygen levels providing new insights into the metabolic adaptations required for haloarchaeal denitrification under changing environmental conditions.

Key points

- O_2 and Fe availability forces dynamic changes in intracellular transition metal pools.
- SirR influences intracellular accumulation of metals in *Haloferax mediterranei*.
- Cell growth phase affects intracellular metals concentration.

Introduction

Denitrification is one of the main processes of the global biogeochemical nitrogen cycle. In this pathway, nitrate is reduced to dinitrogen under anoxic conditions through a series of redox reactions catalysed by four metalloenzymes: nitrate, nitrite, nitric oxide and nitrous oxide reductases. A diverse range of microorganisms utilize this pathway either as a dissimilatory process to dissipate excess of reductant power or as an alternative respiration to oxygen-based respiration (Kuypers et al. 2018).

Over the past few years, denitrification has undergone a comprehensive investigation at various levels, spanning from molecular mechanisms to its global ecological impact. This interest is primarily attributed to its implications in fields such as agriculture, wastewater treatment, and climate change. Regarding the latter, the release of volatile nitrogen intermediates, particularly nitrous oxide (N_2O), is a critical driver of global warming and ozone layer depletion, making the understanding of denitrifying pathways a priority for biosphere health (Erisman et al. 2008; Galloway et al. 2008; Bakken et al. 2012; Bergaust et al. 2012; Stocker et al. 2013; Wang et al. 2021). However, there are still aspects of the denitrification pathway that

remain insufficiently explored, such as the role of denitrifying haloarchaea in extreme conditions (Torregrosa-Crespo et al. 2016). While the biochemistry and the physiology of this process in haloarchaea are well described, the molecular machinery regulating the adaptation of the cell to denitrifying conditions is largely unknown (Torregrosa-Crespo et al. 2019; Torregrosa-Crespo et al. 2020a; Torregrosa-Crespo et al. 2020b). In a previous study, employing RNA-Seq technology, it was described that *Haloferax mediterranei* undergoes important transcriptomic changes when respiring nitrate in the absence of molecular oxygen (Miralles-Robledillo et al. 2024). Remarkably, one of the most interesting findings was that metal homeostasis is widely controlled under denitrifying conditions. This was unveiled through a comprehensive examination of the expression levels of some genes related to iron, copper, molybdenum, and zinc, which exhibited significant differences. These genes encode proteins involved in metal transport, siderophore biosynthesis, and metal delivery processes. Nonetheless, the most significant finding was that a metal-dependent transcriptional regulator from the DtxR family, identified as a SirR repressor (so-called MntR; NCBI Gene ID: E6P09_18060), showed a strong upregulation under denitrifying conditions ($\log_2$ Fold Change = 6.05). Intriguingly, other DtxR regulators of different types are encoded in the *Hfx. mediterranei* genome, but they did not show significant changes in their expression levels under denitrifying conditions. These regulators are of the types SirR (NCBI Gene ID: E6P09_06970), TroR (NCBI Gene ID: E6P09_07185) and Idr (NCBI Gene ID: E6P09_17320) (Miralles-Robledillo et al. 2024).

The DtxR family of transcriptional regulators is one of the two families involved in the homeostasis of iron, manganese, and zinc in prokaryotes (Leyn and Rodionov 2015). Historically, the DtxR family was primarily associated with the control of the *tox* operon involved in the biosynthesis of toxins in *Corynebacterium diphtheriae* in response to iron levels (Tao et al. 1994; Parveen et al. 2019). Nonetheless, further investigations revealed that these regulators exhibit the capacity to bind other divalent metals as ligand molecules such as Zn^{2+}, Co^{2+}, Ni^{2+}, Cd^{2+}, or Mn^{2+} (Golynskiy et al. 2006; Granger et al. 2013; Parveen et al. 2019).

The mechanism of action of these regulators is to interfere with RNA polymerase, preventing it from binding to the promoter region, which categorizes them as repressors (Tao and Murphy 1992; Schmitt 2002). The binding sequences recognized by DtxR regulators exhibit a high degree of conservation across various archaeal species (Leyn and Rodionov 2015). Furthermore, it has been documented that distinct DtxR regulators possess the capability to interact with promoters of genes that encode other members of the DtxR regulatory family, consequently forming intricate regulatory networks (Schmid et al. 2011; Martinez-Pastor et al. 2017).

The DtxR regulons within Archaea encompass the FetR, MntR and ZntR regulons, which regulate the homeostasis of iron, manganese and zinc ions, respectively. Each of these regulons includes distinct sets of genes primarily associated with transporters and uptake systems, including siderophores (Leyn and Rodionov 2015). It should be noted that some of these genes coincide with those that displayed differential expression patterns under denitrifying conditions in the RNA-Seq study mentioned previously (Miralles-Robledillo et al. 2024). Consequently, it raises the possibility that the mentioned SirR repressor

that displayed an upregulation under denitrifying conditions functions as a key transcriptional factor governing the expression of these genes during the transition to anoxia, where low oxygen levels trigger the denitrifying pathway.

To investigate this regulatory link, the present study characterizes the functional role of the SirR regulator through the generation of *sirR* deletion and overexpression strains. Physiological studies were conducted to analyse the growth and intracellular metal concentration of both control and modified strains under conditions of iron and oxygen availability or deficiency. Additionally, the gene expression levels of an ABC transporter iron-binding like protein (NCBI Gene ID: E6P09_00145), an iron-ABC transporter like permease (NCBI Gene ID: E6P09_02480) and the *sirR* gene (NCBI Gene ID: E6P09_18060) were analysed using qRT-PCR across the three strains under both iron-supplemented and iron-limited conditions. Members of the ABC transporter iron-binding protein family are typically part of ABC transporter complexes and function as periplasmic binding proteins. They bind iron complexes and then deliver these complexes to membrane-bound permeases for transport into the cytoplasm (Locher et al. 2002; Ma et al. 2009; Schalk and Guillon 2013). Finally, the SirR regulator was purified, and its molecular mass and quaternary structure were determined using gel filtration chromatography, confirming a homodimeric conformation of SirR in solution, consistent with other characterised members of the DtxR family.

This study aims to elucidate the regulatory effects of iron, oxygen, and the repressor SirR on metal homeostasis and their intracellular accumulation using *Hfx. mediterranei* as a model organism to study denitrification in haloarchaea. Connections with microaerobic and anaerobic respiration are also discussed, thus shedding light on the role of metals as electron donors and enzymatic cofactors during haloarchaeal denitrification.

Materials and methods

Culture media and culture conditions

Hfx. mediterranei strains (HM26 (Pedro-Roig et al. 2013), HM26-Δ*sirR* and HM26-OE*sirR*) were cultivated in a defined medium comprising 27.75 mM glucose, 1 mM Pi (K_2HPO_4/KH_2PO_4), 15 mM NH_4Cl (as a nitrogen source), 10 mM KNO_3 (as an electron acceptor), 2.67 M NaCl, 0.16 M $MgSO_4 \cdot 7H_2O$, 0.133 M $MgCl_2 \cdot 6H_2O$, 53.33 mM KCl, 1.6 mM $NaHCO_3$, 4.53 mM NaBr, 6.6 mM $CaCl_2$, and buffered with 0.1 M (MOPS) (Rodriguez-Valera et al. 1983; Miralles-Robledillo et al. 2023). Additionally, some media were supplemented with 0.005 g/L $FeCl_3$ or 0.005 g/L $FeCl_2 \cdot 4H_2O$, depending on the culture conditions. Furthermore, all strain cultures were also supplemented with 0.45 mM uracil since they are auxotrophic for this nucleotide. The pH of the cultures was adjusted to 7.3 using a 6M NaOH solution.

Aerobic cultures were set up at 42 ºC on a rotary shaker (170 rpm - Infors HT Multitron) in Erlenmeyer flasks with an air chamber that exceeded the culture volume by tenfold. Conversely, anaerobic cultures were set up in 50 mL conical tubes without an air chamber and were grown at 42 ºC without agitation.

Cell growth was monitored spectrophotometrically by measuring the optical density value at 600 nm (OD_{600}). Cultures and OD_{600} determinations were performed in triplicate.

Deletion mutant construction (HM26-Δs irR)

HM26-Δ*sirR* strain was constructed through the targeted deletion of the E6P09_18060 gene (NCBI Gene ID), which encodes the SirR regulator, employing the pop-in/pop-out methodology previously described for *Hfx. mediterranei* (Allers et al. 2004; Pedro-Roig et al. 2013). The construction involved the utilization of the vector pMH101-N (suicide plasmid) and the uracil auxotrophic strain HM26 (Δ*pyrF*) (Supplementary Fig. 1).

First, two overlapping fragments of approximately 500 bp of the sequences flanking the *sirR* gene were amplified by PCR using the primers listed in Supplementary Table 1. The PCR fragments were purified with the GFX PCR DNA and Gel Band Purification Kit from Cytiva and ligated by fusion PCR (Supplementary Fig. 2A and 2B). In the fusion PCR, the two overlapping fragments were aligned, extended and subsequently amplified using primers 1F_18060 and 2R_18060. The result was a 1068 bp fragment, a product of the ligation of the flanking sequences of the *sirR* gene.

*Eco*RV restriction enzyme (Thermo Fisher Scientific) was then used for pMH101-N digestion, and the 1068 bp PCR product obtained from the fusion PCRs was ligated into the linearised plasmid using T4 DNA ligase (Thermo Fisher Scientific) according to the manufacturer's guidelines. The plasmid harbouring the insert was then transformed into *Escherichia coli* DH5α by the heat-shock method. Ampicillin-resistant cells were selected, and the recombinant plasmid was isolated using the E.Z.N.A.® Plasmid DNA Mini Kit I. The correct construction of the recombinant plasmid was verified by PCR (using primers 1F_18060 and 2R_18060; Supplementary Table 1) and Sanger sequencing (using primers pMH101NF_Seq and pMH101NR_Seq; Supplementary Table 1). Once the correct construction was confirmed, the plasmid was transformed into *E. coli* JM110, to obtain a non-methylated vector, which was purified (E.Z.N.A.® Plasmid DNA Mini Kit I) and, after validation of the construction, used for transformation in *Hfx. mediterranei* using the PEG-mediated protocol established for haloarchaea in previous studies (Dyall-Smith 2008).

Verification of recombinants (pop-ins) was carried out in defined medium without uracil and without KNO_3. These recombinants present the wild-type and the deleted version of *sirR*. For the selection of cells devoid of the *sirR* gene (pop-outs), pop-ins were subcultured in defined media in the presence of uracil and 5-fluoroorotic acid (5-FOA). 5-FOA is toxic for cells carrying out the *pyrE2* gene (present in the pMH101-N plasmid). Thus, cells that underwent a second homologous recombination event may result in either reconstitution of the wild-type allele or deletion of *sirR* gene.

The verification of the deleted version in colonies from the pop-out cultures was conducted through PCR using two primer pairs (1F_18060-2R_18060 and pTA1992F_18060-pTA1992R_18060; Supplementary Table 1) designed to amplify distinct regions encompassing the deletion. The hybridization sites and primer sequences are indicated in Supplementary Table 1. All PCRs performed in this work were carried

out using Phusion™ High-Fidelity DNA Polymerase (Thermo Fisher Scientific). The PCR result was checked by agarose gel (TAE 1%).

Following verification, cultures exhibiting a PCR product consistent with the *sirR* deletion underwent multiple subculturing cycles, alternating between defined media lacking uracil and defined media lacking both uracil and phosphate. This protocol aimed to diminish the chromosomal copy number by subjecting cells to a phosphate deficiency (Zerulla et al. 2014). After each subculture cycle, PCR verification was systematically performed until homozygosity for the deletion was identified.

Homologous overexpression strain construction (HM26-OE sirR)

The overexpression strain HM26-OE*sirR* was constructed using the pTA-1992 plasmid, generously provided by Dr. Thorsten Allers (University of Nottingham) (Supplementary Fig. 3) (Haque et al. 2019; Haque et al. 2020). First, the E6P09_18060 gene was amplified by PCR using primers designed to introduce *Bsp*HI (Thermo Fisher Scientific) and *Bam*HI (Thermo Fisher Scientific) restriction sites (pTA1992F_18060 and pTA1992R_18060 primers; Supplementary Table 1). Subsequently, the pTA-1992 plasmid was subjected to restriction with the same enzymes, and the resulting digested products were ligated using T4 DNA ligase according to the manufacturer's specifications. The resulting construct contains the *sirR* gene with an additional histidine tag in the N-terminus, under the control of a strong synthetic promoter (designated as *p.syn*) (Haque et al. 2019; Haque et al. 2020). Transformation procedures were carried out according to the methodology outlined in the previous section. The correct construction was validated by PCR and Sanger sequencing after the isolation of the plasmid from transformed cells. All PCRs performed in this work were carried out using Phusion™ High-Fidelity DNA Polymerase (Thermo Fisher Scientific).

Metal content analyses

Hfx. mediterranei HM26, the control strain, was first analysed at different growth phases and O_2 conditions in culture media supplemented with $FeCl_3$ to study the effect of iron on cell growth and intracellular metal concentrations. Early and late growth phases were defined as follows: early growth corresponded to an OD_{600} of 0.2 for oxic cultures and 0.6 for denitrifying cultures, while late growth corresponded to an OD_{600} of 4.5 for oxic cultures and 1.0 for denitrifying cultures (Miralles-Robledillo et al. 2023). These last values correspond to the stationary phase of both oxic and anoxic cultures. Following this initial analysis, intracellular metal concentrations in the control and engineered strains (HM26-Δ*sirR* and HM26-OE*sirR*) were measured exclusively at the stationary phase for comparison under different culture conditions.

For this purpose, approximately 50 mL of stationary phase cultures were centrifuged at 7,200 x g for 30 minutes at 4 ºC. The resulting supernatant was diluted 5 times with mQ-H_2O and stored at 4°C until analysis, and the pellet was washed twice with an autoclaved solution consisting of 2 M NaCl, 0.12 M $MgSO_4{\cdot}7H_2O$, 0.102 M $MgCl_2{\cdot}6H_2O$, 40.241 mM KCl, 1.19 mM $NaHCO_3$, 3.402 mM NaBr 4.955 mM $CaCl_2$.

Following each wash, centrifugation was performed at 7,200 x g for 30 minutes at 4 ºC. The washed pellet was then dried in an oven at 50 ºC for 64 hours.

The dried pellets and the diluted supernatant were sent to the Technical Research Services (SSTTI) at the University of Alicante for inductively coupled plasma mass spectrometry analysis (ICP-MS) to quantify iron, manganese, copper, zinc, and molybdenum. Firstly, pellets were subjected to acid digestion. The pellets were weighed and introduced into acid-washed 15 mL quartz digestion vials fitted with Teflon-lined caps. Subsequently, 4 mL of HNO_3 was added to initiate the digestion process. Digestion was performed using the Milestone ultraWAVE digestion system. The temperature program used for the microwave digestion included a 5-minute ramp from room temperature to 100°C, 15 minutes at 100°C to 170°C, 10 minutes from 170°C to 240°C, and finally, 15 minutes at 240°C. Post-digestion, the samples were diluted to a final volume of 15 mL with mQ-H_2O and subjected to ICP-MS analysis.

For ICP-MS analyses of digested pellets and diluted supernatants, calibration standards were prepared using different concentrations of Plasmacal SCP MS 33 10 (SCP Science) solution. A final concentration of 2% HNO_3 was employed for the calibration standards used for the quantification of the pellets. An Agilent ICP-QQQ 8900 inductively coupled plasma mass spectrometer triple quadrupole was employed for the analyses. The instrument was used with a helium (He) collision cell to eliminate possible spectral interferences caused by the reaction of the argon gas (Ar) with the analytes. The parameters used in the equipment are listed in Table 1. MassHunter Software (Agilent) was utilized for data processing, enabling the determination of the total concentration of the selected elements in the sample solutions.

Table 1
Parameters used for the elemental analysis (Agilent ICP-QQQ 8900)

Parameter (Units)	**Value**
Radiofrequency power (W)	1550
Ar flow (L/min)	1.09
He flow (ml/min)	5
Sample uptake (mL/min)	0.3
Sampling depth (mm)	10
Sweeps	100
Replicates	3
Dwell time (s)	0.3
Spray chamber temperature (°C)	2

RNA extraction and qRT-PCR analysis

A starting number of 5×10^8 cells (estimated by measuring the OD_{600} value, assuming that an OD_{600} value of 1 corresponds to 1.8×10^8 cells/ml; this correlation between cells and OD_{600} values was previously established in the laboratory) served as the initial substrate for RNA extraction, employing the QIAGEN RNeasy Kit (Invitrogen). Samples were taken in the stationary phase at the same time as the ICP-MS samples taken at this point. However, in this case, only iron-limited cultures and cultures supplemented with $FeCl_3$ were analysed (not samples supplemented with $FeCl_2 \cdot 4H_2O$). RNA from each sample was treated with the TURBO DNA-free kit (Invitrogen): 600 ng of RNA sample was digested in a 10 µL reaction with 3 Units (U) of TURBO DNAse. Samples were first incubated with 1.5 U of TURBO DNAse for 1 hour at 37 ºC, then a further 1.5 U were added, and the sample was incubated for a further hour.

Reverse transcription of 300 ng of the digested RNA samples was carried out using the SuperScript™ VILO™ MasterMix kit (Invitrogen) to obtain cDNA. A further 300 ng was used as a negative retrotranscriptase control. The manufacturer's instructions were followed for this step.

The samples from the preceding step were subjected to amplification using the RT-PCR SuperScript™ VILO™ MasterMix (Invitrogen). The housekeeping reference genes selected were 16s rRNA (NCBI Gene ID: E6P09_RS12125 and E6P09_RS02595; there are two copies of the gene in the genome) and the gene encoding cytochrome *b* subunit of the cytochrome *bc* complex (NCBI Gene ID: E6P09_07090), both genes showed constitutive expression in the transcriptomic comparations of oxic and anoxic conditions and have been used previously as reference genes in other studies (Lledó et al. 2004; Weltzien et al. 2005; Feng et al. 2013; Miralles-Robledillo et al. 2024) The reference genes were validated before further analyses. Two genes encoding iron transporters were targeted to analyse their expression across all study conditions (NCBI ID: E6P09_00145 and E6P09_02480; designated in this study as ABC transporter iron-binding like protein and iron-ABC transporter like permease, respectively). These genes were selected from the list of genes displayed in Supplementary Table 2, the expression of which was considered likely to be regulated by SirR (based on the previous RNA-Seq study) (Miralles-Robledillo et al. 2024). E6P09_02480 was the only gene encoding a transmembrane subunit of an ABC type iron transporter and the E6P09_00145 gene was selected among the other genes encoding periplasmic proteins related to iron ABC transporters. Detailed primer information is provided in Supplementary Table 3. The efficiency of the amplification was calculated using five serial dilutions of the cDNA samples. The strain HM26, grown in oxic cultures supplemented with iron, was used as a control for the normalization. The normalized fold expression of the target genes was computed employing the methodology outlined by Fenrich and colleagues (Taylor et al. 2019). All conditions studied had three biological replicates and two technical replicates analysed by qPCR.

The qPCRs were run in a StepOnePlus™ Real-Time PCR System (Applied Biosystems). The program used for amplification included a melting curve step to check for correct amplification. Details of the program are given in Supplementary Fig. 4.

Statistical analysis of the intracellular metal content and qRT-PCR Normalized Fold Expression Values

Data analysis was performed using R statistical software. To explore patterns and trends in the dataset, a Principal Components Analysis (PCA) was first conducted, with the intracellular metal concentrations measured by ICP-MS as variables. This initial analysis informed the design of subsequent statistical tests.

A Bartlett's test of homogeneity of variances was applied to both the intracellular metal concentrations and the qRT-PCR Normalized Fold Expression Values. Homogeneity of variance was observed for all datasets except for the initial ICP-MS analysis of the control strains under different growth phases and oxygen conditions (Supplementary Table 4). Consequently, this specific dataset was analysed using the non-parametric Kruskal–Wallis test, while all other datasets were analysed using Analysis of Variance (ANOVA).

A three-way ANOVA was performed to assess the variation in intracellular metal concentrations across the three strains and culture conditions during the stationary phase. The factors included in the analysis were: strain (HM26, HM26-Δ*sirR* or HM26-OE*sirR*), iron supplementation or not, and oxic or anoxic conditions. Each metal was analysed individually, except for iron. For iron, a separate ANOVA was conducted for iron-supplemented and iron-limited cultures due to the substantial differences observed in intracellular iron content between these two conditions, with supplemented cultures showing markedly elevated values and limited cultures showing significantly lower values. For all comparisons, the significance level (α) was set at 0.05.

When significant differences were detected via ANOVA, Tukey's Honestly Significant Difference (HSD) test was used as a post hoc analysis to identify specific variations among the experimental conditions. The significance level (α) remained at 0.05 for all post hoc comparisons.

The same ANOVA and post hoc analyses were applied to the qRT-PCR Normalized Fold Expression Values for the genes encoding the iron transporters and the SirR regulator.

Promoter region analyses of iron-related genes

The sequences of the promoter regions of iron-related genes exhibiting significant negative expression changes under denitrifying conditions in the previous RNA-seq analysis were used to identify common regulatory motifs in their nucleotide sequence (Miralles-Robledillo et al. 2024). The list of these genes is shown in Supplementary Table 2. The bioinformatic tool MEME from the online tool MEME-Suite 5.5.4 was utilised for this purpose (Bailey et al. 2015). Default parameters were applied for the analysis. The motif found with MEME was used to perform a manual search for similar motif repeats in the same promoters. The motif found was represented as a logo using WebLogo (Schneider and Stephens 1990; Crooks et al. 2004). In these analyses, all the spaces between two coding regions were considered

promoter regions. The promoter sequences were acquired from the National Center for Biotechnology Information (NCBI) Gene database (Sayers et al. 2023).

Protein purification

Protein extracts were prepared as follows to facilitate the subsequent purification of the His-tagged SirR regulator. A 500 mL aerobic cell culture was cultured for 48 hours as previously described. Cells were harvested by centrifugation of the culture at 25,000 x g for 30 minutes at 4°C. The resulting pellet was collected and resuspended to a 30% (w/v) concentration in a buffer containing 1.5 M NaCl, 20 mM HEPES (4-(2-hydroxyethyl)-1-piperazineethanesulfonic acid), 1 mM PMSF (phenylmethylsulphonyl fluoride, protease inhibitor) at pH 7.2. This mixture was sonicated until the solution was no longer turbid and centrifuged at 50,000 x g for 1 hour at 4°C. The supernatant was collected, and the protein concentration was measured using the Qubit Protein Broad Range Assay (Invitrogen).

The His-tagged SirR (His_6-SirR) was purified from the protein extracts using 5 mL HisTrap columns (Cytiva) containing nickel, in an ÄKTA Start system. The column was initially equilibrated and washed with 5 CV (Column Volumes) of 1.5 M NaCl and 20 mM HEPES buffer at pH 7.2, at a flow rate of 1 mL/min. The sample application was performed under the same flow rate conditions. Elution was performed using an elution buffer of 500 mM imidazole, 1.5 M NaCl, and 20 mM HEPES, at pH 7.2, at a flow rate of 0.5 mL/min. The elution protocol included the following steps: 4 CV of 1% elution buffer; 4 CV from 1% to 4% elution buffer; and 8 CV from 4% to 100% elution buffer.

Absorbance at 280 nm was continuously measured in the UV flow cell of the ÄKTA Start system. Fractions of 2 ml were collected, and the protein concentration of the fractions of interest was determined by Qubit Protein Broad Range Assay (Invitrogen) and further analysed by 12% denaturing polyacrylamide gel (SDS-PAGE). Following electrophoresis, gel bands corresponding to the molecular weight of the SirR regulator were subjected to trypsin digestion and subsequently analysed using mass spectrometry (nano-HPLC-1100/IT XCT plus, Agilent) to confirm the identity of the purified protein. The software utilized for mass spectrometry analyses was Spectrum Mill (Agilent). The analytical process was conducted at the Technical Research Services (SSTTI) of the University of Alicante. Fractions containing the proteins were mixed and concentrated using a Vivaspin® 20 Centrifugal Concentrator.

The concentrated protein was further purified, and the molecular weight was determined in its native monodisperse state employing a HiPrep 16/60 Sephacryl S-100 HR column on the ÄKTA Start system. Column equilibration, washing, and elution were conducted using a buffer of 1.5 M NaCl, 20 mM HEPES at pH 7.2, with a flow rate of 0.5 mL/min. The column calibration to determine molecular weight was performed using cytochrome c, carbonic anhydrase, albumin, and blue dextran from the Gel Filtration Markers from the MWGF200 Kit (Sigma-Aldrich), according to the instructions of the manufacturer (Supplementary Fig. 5). The determination of protein concentration and examination of fractions were performed as described above.

Results

Altered sirR expression differentially affects growth depending on iron and oxygen

To investigate the physiological role of the SirR regulator under different environmental conditions, the growth of the control strain HM26, the deletion mutant HM26-Δ*sirR*, and the overexpression strain HM26-OE*sirR* was monitored to determine whether iron levels, together with the availability or absence of oxygen, influenced their growth (Fig. 1). Under aerobic conditions with iron supplementation, similar growth profiles were obtained using Fe^{2+} or Fe^{3+} as the iron source., and the major differences were observed in the HM26-OE*sirR* strain (Fig. 1A, 1B). Whereas the control and HM26-Δ*sirR* strains showed a very similar growth curve in the presence of both iron and oxygen, the HM26-OE*sirR* showed a longer lag phase (approximately 30 hours) and reached lower maximum OD_{600} values compared to the other strains.

Under anoxic conditions with iron supplementation (Figs. 1D, 1E), all strains exhibited diauxic growth, caused by the shift to anoxic conditions, which led to a secondary adaptation phase. As observed under aerobic conditions, HM26-OE*sirR* showed a longer adaptation phase and reached a lower maximum OD_{600} values compared to the other strains (Figs. 1D, 1E). However, in contrast to the results obtained under aerobic conditions, HM26-Δ*sirR* also reached a lower maximum OD_{600} than HM26 (Figs. 1D, 1E). Thus, both deletion and overexpression of *sirR* affected growth under anoxic, iron-supplemented conditions, although the effect was more pronounced in the overexpression strain.

Under iron limitation conditions, the cultures showed a longer time to reach the stationary phase and an increased variability among biological replicates than cultures with iron supplementation (Figs. 1C, 1F). The most notable changes occurred in aerobic cultures, where the HM26-OE*sirR* strain exhibited better adaptation (short lag phase and OD_{600} values higher than the other strains) (Fig. 1C), contrary to the observations in aerobic cultures with iron supplementation (Figs. 1A, 1B). Conversely, the HM26-Δ*sirR* strain showed a higher susceptibility, reaching the lowest maximum OD_{600} value (Fig. 1C). Finally, under oxygen-depleted and iron-limited conditions (Fig. 1F), the maximum OD600 values were similar to those reached by each strain under anaerobic conditions with iron supplementation. However, these values were reached later, suggesting that the trace amounts of iron present in the salts used to prepare the medium may be sufficient to support growth under anoxic conditions

Intracellular metal accumulation depends on the growth phase

To establish a physiological baseline of metal dynamics, the intracellular metal concentrations in the control strain HM26 at early and late growth phases under oxic and denitrifying conditions were determined by ICP-MS. Initial analysis using the non-parametric Kruskal-Wallis test, revealed that only molybdenum levels were significantly affected by oxygen availability. In contrast, the concentrations of manganese, iron, copper, and zinc were primarily influenced by the growth phase (Fig. 2; Supplementary Tables 5 and 6).

Specifically, the early growth phase exhibited higher intracellular metal accumulation compared to the late (stationary) phase. Iron content was particularly notable, as it showed the highest accumulation among the measured metals. Iron was also the most abundant metal in the culture medium (~ 200 ppb), with concentrations approximately 2.5 times higher than manganese and 4 times higher than copper (Supplementary Fig. 6). However, intracellular iron levels in the cells during the early growth phase were significantly higher than those observed in the extracellular medium, indicating a substantial intracellular enrichment.

A similar pattern was observed for zinc (Supplementary Fig. 6). Despite its lower extracellular concentration relative to iron, manganese, and copper, zinc was the second most abundant intracellular metal measured during the early growth phase. This result suggests that intracellular zinc levels are not determined solely by its extracellular availability and may reflect an increased cellular requirement during active growth.

Oxygen availability and SirR overexpression influence intracellular metal levels during stationary phase

After characterizing metal dynamics in the control strain across different growth phases, subsequent analyses focused specifically on the stationary phase. This approach allowed a systematic and comparable evaluation of how sirR deletion and overexpression alter the homeostasis of intracellular metal pools under the distinct conditions tested.

Intracellular iron, manganese, copper, zinc, and molybdenum concentrations were measured by ICP-MS in the three strains grown under oxic or anoxic conditions, either without iron supplementation or supplemented with Fe^{2+} or Fe^{3+} (Fig. 3). The resulting dataset was analysed by principal component analysis (PCA). PCA served as a tool for data visualization when a high number of observations were made with different variables. The results extracted from the PCA were robust, as indicated by the scree plot showing that the two analysed dimensions explain 84.9% of the variance of the observations (Supplementary Fig. 7).

PCA showed a clear separation according to oxygen availability. One cluster comprised samples grown under oxic conditions, located on the left side of the PCA biplot (Fig. 3, filled figures), while another cluster consisted of samples grown under anoxic conditions, located on the right side of the PCA biplot (Fig. 3, empty figures). Notably, the latter cluster exhibited a positive correlation with the variables, suggesting elevated intracellular metal concentrations. This pattern was consistent with generally higher intracellular metal concentrations under anoxic conditions. Samples grown without iron supplementation also tended to separate from iron-supplemented cultures along dimension 2 of the PCA (Fig. 3, circles). Across all these delineated groups, it was observed that the HM26-OE*sirR* overexpression strain consistently exhibited a higher positive correlation with the metal concentration compared to the other strains under the same conditions (Fig. 3, orange figures). This pattern suggested that SirR overexpression was associated with increased intracellular metal levels. Finally, no clear separation was

determined for samples supplemented with Fe^{2+} or Fe^{3+}, suggesting that the form of iron was not a relevant factor in the analysis.

ANOVA revealed that intracellular metal accumulation was significantly influenced by the three selected factors: strain, iron supplementation, and oxygen availability, although the magnitude and significance of these effects differed among metals (Supplementary Table 8). Significant interactions among the three factors were detected for iron, manganese, copper, and molybdenum. Zinc was the only metal for which the three-way interaction was not significant, although a significant interaction between oxygen availability and iron supplementation was observed (Supplementary Table 8). To refine these findings, Tukey's post hoc test was performed for pairwise comparisons.

For manganese accumulation (Fig. 4A), Tukey's test showed that only the HM26-OE*sirR* overexpression strain showed significant accumulation compared to the control and HM26-Δ*sirR* deletion strain (Supplementary Table 9). Anoxic growth was also associated with increased manganese levels, particularly in cultures supplemented with Fe^{2+} or Fe^{3+}, contrary to the iron-limited conditions, where no differences were found (Supplementary Tables 10 and 11).

An exception was detected in the control strain under oxic conditions, in which cultures without iron supplementation showed higher intracellular manganese concentrations than iron-supplemented cultures. This result suggests that manganese homeostasis may be affected by iron availability under specific conditions, although the underlying mechanism remains unclear. Regarding the oxidation state of iron, there were no significant changes in manganese accumulation (Supplementary Table 12).

As mentioned, intracellular iron concentration (Fig. 4B) showed a significant difference among the three strains. In general, the HM26-OE*sirR* overexpression strain showed higher accumulation than the other strains under iron-supplemented conditions, independently of the oxygen levels (Supplementary Tables 13, 14 and 15).

Anoxic growth was associated with increased intracellular iron in several strain and supplementation combinations (Supplementary Tables 15 and 16). Significant increases were detected for HM26-Δ*sirR* in Fe^{3+}-supplemented cultures and for HM26-OE*sirR* in Fe^{2+}-supplemented cultures. A similar trend was observed for HM26-OE*sirR* grown with Fe^{3+}, although the strength of the statistical evidence was lower. Intriguingly, under limited iron conditions, this trend was the opposite, and a significant accumulation was shown under oxic conditions (Supplementary Table 8). Finally, Tukey's HSD test did not find differences in the form of iron when it was added to the culture as a supplement (Supplementary Table 8).

Intracellular copper concentrations (Fig. 4C) again exhibited differences among strains using the ANOVA test (Supplementary Tables 8 and 17). However, the *post hoc* analysis showed that there were no significant differences between the modified and control strain HM26 under the same conditions. Only small p-values (< 0.1) were obtained for the HM26-OE*sirR* overexpression strain in some cases (Supplementary Table 18).

In contrast, oxygen availability had a marked effect on copper levels. All conditions tested demonstrated a significant increase in copper accumulation in anoxic conditions with respect to oxic conditions. The only exception was the control strain grown without iron supplementation, for which no significant difference was observed (Supplementary Tables 19 and 20).

Once again, the oxidation state of iron was not identified as a significant factor influencing the accumulation of copper (Supplementary Table 21). Nevertheless, disparities in copper accumulation between iron-limited and supplemented conditions were observed. Specifically, the control strain HM26 exhibited higher copper levels under oxic conditions with limited iron than under anoxic iron supplemented conditions (Supplementary Table 17).

Zinc accumulation (Fig. 4D) showed a distinct pattern, as no significant three-way interaction among strain, iron supplementation, and oxygen availability was detected (Supplementary Table 8). However, zinc concentrations were influenced by the interaction between oxygen availability and iron supplementation. HM26-OE*sirR* overexpression strain showed higher zinc accumulation compared to the control strain (Supplementary Table 22). Nonetheless, under the same experimental conditions, these differences were generally small and were not consistently significant. In contrast, oxygen availability appeared to play a major role in zinc accumulation. Specifically, anoxic cultures supplemented with Fe^{2+}or Fe^{3+} exhibited increased zinc concentrations (Supplementary Tables 23 and 24).

In iron-limited cultures, no significant differences in zinc accumulation were observed between oxic and anoxic conditions. The oxidation state of the added iron did not significantly influence zinc levels (Supplementary Table 8).

Molybdenum exhibited the lowest intracellular concentration among all the measured metals (Fig. 4E). Regarding inter-strain comparisons, trends like those observed for other metals were noted, with the HM26-OE*sirR* overexpression strain showing significantly higher molybdenum accumulation than the HM26 strain under specific conditions (Supplementary Table 25). Specifically, significant differences were detected between the HM26 and the HM26-OE*sirR* overexpression strain in oxic cultures supplemented with Fe^{3+}, and in anoxic cultures supplemented with ferrous iron Fe^{2+}.

Oxygen availability profoundly affects molybdenum levels. All three strains showed significantly higher intracellular molybdenum concentrations under anoxic conditions when the medium was supplemented with either Fe^{2+} or Fe^{3+}. (Supplementary Tables 27 and 28). However, in iron-limited cultures, this anoxia-induced increase was not statistically significant (Supplementary Table 28).

Remarkably, molybdenum was the sole metal exhibiting significant differences in its concentration between cultures supplemented with Fe^{3+} or Fe^{2+} in some comparisons (Supplementary Table 29). Specifically, differences were found comparing anoxic cultures of the HM26 strains supplemented with iron (Supplementary Table 30). Nevertheless, because molybdenum concentrations were close to the lower range of detection, these differences should be interpreted cautiously.

Finally, a significant reduction in molybdenum accumulation was observed when comparing iron-limited cultures against iron-supplemented cultures across most comparisons (Supplementary Table 31), particularly under anoxic conditions.

In summary, metal accumulation patterns in stationary-phase cultures were primarily influenced by oxygen availability, with significantly higher metal concentrations observed under anoxic conditions. Regarding the strain factor, the HM26-OE*sirR* overexpression strain consistently exhibited greater metal accumulation than both the deletion and control strains. By contrast, the HM26-Δ*sirR* strain generally showed metal profiles like those of the control strain under the conditions tested.

The use of Fe^{3+} or Fe^{2+} in the cultures had a limited effect on metal homeostasis. These results align with the growth curve observations, where the HM26-OE*sirR* overexpression strain demonstrated the most affected growth phenotype, and no significant differences were observed between cultures supplemented with different iron forms.

Finally, the presence or absence of iron supplementation had varying effects depending on the specific metal analysed. Manganese, copper, and zinc levels tended to increase in certain cultures without iron supplementation, whereas molybdenum accumulation decreased under low-iron conditions.

The gene expression of the proteins involved in iron transport is dependent on iron, oxygen and SirR

To determine whether the observed changes in intracellular iron accumulation were associated with transcriptional control of metal uptake systems, the expression of genes encoding two putative iron transport proteins was analysed by qRT-PCR (Fig. 5; Supplementary Table 32). These analyses were not performed on cultures supplemented with Fe^{2+} as physiological analyses showed that there were no major differences depending on the oxidation state of the supplemented iron. The acquired data were normalised with two reference genes. Greater variability among biological replicates was observed in cultures without iron supplementation, as previously noted for the growth curves. Relative gene expression was calculated relative to the HM26 strain under iron-supplemented and oxic conditions, which is the control condition and served as the calibrator.

For the gene encoding the ABC transporter iron-binding like protein (E6P09_00145), ANOVA revealed that iron supplementation significantly influenced its expression (Supplementary Table 33). However, the individual factors of strain and oxygen were not statistically significant. Interestingly, interactions between these factors and iron showed varying degrees of importance. While the interaction between strain and iron showed a non-significant trend ($p = 0.06955$), the interaction between oxygen and iron was highly significant ($p = 0.00263$). The relative expression of the gene encoding the ABC transporter iron-binding like protein increased in the three strains under conditions of oxygen and/or iron limitation, indicating a positive regulatory response to these restrictions. This increase was statistically significant under iron-limited conditions and iron-limited conditions combined with anoxia (Fig. 5; Supplementary Tables 34, 35, and 36). These results indicate that the transcriptional response of the gene encoding

ABC transporter iron-binding like protein was primarily associated with the absence of iron supplementation and was modulated by oxygen availability

No statistically significant differences were detected among strains grown under the same conditions, in part due to high biological variability, but a clear trend was observed (Supplementary Table 37). Under iron-limited conditions and iron-limited conditions combined with anoxia, the HM26-OE*sirR* overexpression strain consistently exhibited the lowest expression levels, whereas the deletion mutant displayed the highest expression levels (Fig. 5). These data suggest that the transcriptional repressor SirR may be involved in the regulation of this gene.

In contrast, the gene encoding the iron-ABC transporter like permease (E6P09_02480) exhibited a distinct regulatory pattern: ANOVA test showed that in the expression of this gene, both iron and oxygen influence independently, but there are no significant interactions (Supplementary Table 33). In this case, the relative gene expression in the three strains decrease significantly under anoxic conditions and increases significantly in the iron-limited culture in the presence of oxygen (Supplementary Table 38, 39). Thus, expression of this gene was negatively regulated by oxygen limitation and positively regulated by iron limitation. Furthermore, in anoxic cultures with iron limitation, the expression levels in HM26 resembled those under control conditions. This result suggests that the stimulatory effect associated with the absence of iron supplementation may be counteracted by the reduction in expression associated with anoxia. Regarding differences among strains, no substantial differences were discerned under the same condition (Fig. 5).

Finally, the expression of *sirR* was analysed in the control strain HM26. In this case, although in the ANOVA test the interaction between iron and oxygen was significant, the individual Tukey contrasts did not detect clear differences between conditions (Supplementary Tables 33 and 40). This outcome may be attributed to a lack of statistical power due to a small sample size or the possibility that the observed effect is subtle under stationary-phase conditions. Notably, intracellular metal concentrations in stationary-phase cultures are considerably lower compared to those in early growth phases, where previous RNA-Seq studies had identified differences in *sirR* expression (Fig. 2) (Miralles-Robledillo et al. 2024).

The promoter regions of iron uptake-related genes share a regulatory motif

To identify potential *cis*-regulatory elements that mediate transcriptional control of iron uptake-related genes, an *in silico* analysis of their upstream regions was performed. The analysis included genes and operons that had shown significant negative $\log_2$ Fold Change values under denitrifying conditions in a previous RNA-Seq study (Miralles-Robledillo et al. 2024). MEME analysis allowed the identification of a shared semi-palindromic motif of 19 nucleotides (Fig. 6A). Moreover, a manual search revealed that the consensus sequence was repeated in some of the analysed promoters with small variations in the sequences. Specifically, the predicted positions for this motif were located between − 1 and − 324 bp

relative to the translational start site (ATG) (Supplementary Fig. 8). These repeats were analysed with the WebLogo tool and are represented by the logo shown in Fig. 6B.

Two repetitions of the consensus sequence were found in the sequence upstream of the operon, including genes E6P09_02485 (encoding a NAD(P)/FAD-dependent oxidoreductase), E6P09_02480 (encoding an iron-ABC transporter like permease), and E6P09_02475 (encoding an ABC transporter ATP-binding protein). Analysis of the previous RNAseq data confirmed that these genes are transcribed in a single transcription unit (Miralles-Robledillo et al. 2024).

Two repetitions of the sequence were also found in the promoter of the operon constituted of genes E6P09_18555 to E6P09_18530 (encoding siderophore biosynthesis genes). The single transcription unit in this operon was also supported by the RNA-seq data.

The promoter of the E6P09_11455 gene (encoding also a member of the ABC transporter iron-binding protein family) exhibited, as well, two repetitions of the consensus sequence. Meanwhile, the promoter of the operon involving E6P09_17310 (encoding another member of the ABC transporter iron-binding protein family) and E6P09_17315 genes (encoding an iron transport protein) showed three repetitions. In contrast, the promoter regions associated with the genes E6P09_00145 (encoding the ABC transporter iron-binding like protein analysed in the present work) and E6P09_12005 (encoding another member of the ABC transporter iron-binding protein family) revealed the presence of only one consensus sequence (Supplementary Fig. 8).

The purified SirR repressor exhibits a homodimeric conformation

Given that the regulatory motif identified in the promoters of iron uptake-related genes displays a semi-palindromic structure, often found in binding sites recognized by dimeric repressors, we next investigated the oligomeric state of purified SirR in solution.

Recombinant His_6-SirR was purified by metal-affinity chromatography followed by size-exclusion chromatography. SDS-PAGE analysis of the purified protein showed that the estimated size for the monomeric form of the regulator is around 30 kDa, which is slightly higher than the *in silico* estimated theoretical mass (26.5 kDa) (Fig. 7). However, this overestimation by SDS-PAGE is common for halophilic proteins, which have an unusual amino acid composition that confer a highly acidic character which may alter SDS binding and electrophoretic mobility (Bonete et al. 1996). Moreover, a highly purified protein fraction was obtained after the two chromatographic steps (Fig. 7). Finally, the analysis of the elution volume of the SirR regulator in gel filtration chromatography (HiPrep 16/60 Sephacryl S-100 HR column) is consistent with a homodimer whose molecular mass is around 59 kDa, according to the calibration curve reported in Supplementary Fig. 5 and the chromatogram shown in Supplementary Fig. 9. These results support the hypothesis that the biologically relevant form of SirR is a homodimer.

Discussion

Haloarchaeal denitrification produces a large set of changes in the cell to adapt the metabolism to a new way of obtaining energy from electron transfer reactions involving nitrate or nitrite (Miralles-Robledillo et al. 2024). These changes include the expression of metalloreductases and electron transport proteins that allow optimal electron fluxes and energy conservation under oxygen-limiting conditions (Torregrosa-Crespo et al. 2020b). Nonetheless, other indirect changes that take place under denitrifying conditions remain less studied, such as the metal homeostasis, a process of particular interest because several enzymes and electron-transfer components involved in denitrification require metal-containing cofactors. The relationship between metal availability, intracellular metal accumulation, and denitrifying metabolism has received limited attention.

One of the few studies addressing this topic was carried out in *Paracoccus denitrificans*, a model microorganism of bacteria in denitrification studies. In this organism, the two-component NrtXY system was found to be involved not only in the regulation of nitrogen metabolism, but also in iron homeostasis. The study revealed that a mutant strain defective in the *ntrY* gene exhibited changes in the expression of several genes related to iron metabolism, approximately 40% lower intracellular iron content compared to the wild-type strain, lower NosZ activity, and increased siderophore production (Olaya-Abril et al. 2022). These observations support the existence of regulatory links between metal homeostasis and nitrate respiration.

Building upon these findings, the present study aimed to explore the regulatory effects of iron, oxygen, and the repressor SirR on metal homeostasis and intracellular metal accumulation in the denitrifying haloarchaeon *Hfx. mediterranei*.

Initial physiological analyses revealed that, under both oxic and anoxic conditions, intracellular metal concentrations per cell were higher during early growth phases than during stationary phases, except for molybdenum (Fig. 2). However, a notable decrease in the intracellular concentration of certain metals, such as iron, was observed between early oxic and early denitrifying cultures. This reduction in iron levels is consistent with previous RNA-Seq data showing that several genes encoding putative iron transporters are downregulated during the early response to denitrification, whereas *sirR* expression is increased (Miralles-Robledillo et al. 2024). These changes in the intracellular metal concentration over time are consistent with another study that examined the accumulation of different metals over time in *Salmonella* typhimurium (Rolfe et al. 2012). In that study, manganese and iron showed higher intracellular concentrations in the lag phase than in the stationary phase, while molybdenum levels remained comparatively stable. Moreover, the genes encoding iron and manganese transporters were upregulated during the lag phase, while molybdenum transport systems showed higher expression during the stationary phase (Rolfe et al. 2012). Fundamentally, the reason behind this accumulation is the requirements of the cells to build the essential machinery (such as cofactors for enzymes) (Iuchi and Weiner 1996; Rolfe et al. 2012). In addition, dilution associated with cell division and biomass accumulation, together with changes in metal efflux, and metabolic utilization, may contribute to the progressive decrease in cellular metal content observed as cultures approach stationary phase.

Physiological analyses during the stationary phase revealed that both overexpression and deletion of the *sirR* gene had a discernible effect on cell growth (Fig. 1). Both modified strains showed impaired growth under oxygen limitation in the presence of iron, (Fig. 1). However, when oxygen was present in the culture, the *sirR* deletion mutant did not show affected growth, whereas the HM26-OE*sirR* overexpression strain remained the most affected. These data agree with the metal accumulation observed in the three strains, where the HM26-OE*sirR* overexpression strain showed significantly higher metal accumulation for the different metals measured over a wide range of conditions tested. (Fig. 4). The observed accumulation of metals may potentially be the underlying factor contributing to the altered growth, indicating that metal uptake and/or the efflux would be affected by *sirR* overexpression. Moreover, this phenomenon could explain the comparatively favourable growth of the HM26-OE*sirR* overexpression strain under iron-deficient conditions (Figs. 1C and 1F), where its greater ability to accumulate metals may contribute to this phenotype by partially compensating for limited iron availability.

The intracellular accumulation of metals on the different strains in stationary phase was more evident under denitrifying conditions (oxygen limitation). This observation is consistent with the increased requirement for specific metal cofactors associated with denitrification enzymes and electron-transfer proteins during anaerobic respiration (Fig. 3) (Torregrosa-Crespo et al. 2020b; Miralles-Robledillo et al. 2024). Nevertheless, the different metals analysed are unlikely to contribute equally to this process, and changes in intracellular concentrations may also reflect broader remodelling of metal homeostasis.

An additional response was observed in iron-deficient cultures grown under aerobic conditions, in which manganese and copper accumulate to a greater extent in the HM26 control strain. This observation could be interpreted as a strategic response by the cell to overcome iron deficiency. Analogously, it has been demonstrated in *Escherichia coli* that manganese can substitute for iron in numerous metalloproteins under such conditions (Martin et al. 2015). Therefore, *Hfx. mediterranei* may favour the uptake of these metals due to iron deficiency, adopting a similar adaptive strategy.

The comparison between transcriptional data and intracellular metal measurements further illustrates the complexity of this regulatory system. Expression levels of the selected iron transport genes measured by qRT-PCR did not show a simple correspondence with the ICP-MS profiles. The heightened metal accumulation observed in the HM26-OE*sirR* overexpression strain under anaerobic conditions, specifically in the presence of Fe^{3+}, in comparison to other strains, is not accompanied by a proportional upregulation of the analysed transporters (Fig. 5). Moreover, minimal disparities in expression levels of the transporters are discernible among strains under these conditions for the genes encoding the transporters (Fig. 5). This lack of direct correspondence is not unexpected, because intracellular metal content reflects the combined contribution of uptake, efflux, or metabolic utilization. Differences in metal efflux regulation among the strains could therefore contribute to the observed accumulation patterns, although this hypothesis remains to be experimentally tested; it provides a compelling direction for future studies to further elucidate the mechanisms of metal homeostasis in *Hfx. mediterranei*.

Despite these discrepancies, the qRT-PCR analyses support a role of SirR in the regulation of the gene encoding the periplasmic substrate-binding protein of the iron ABC transporter (E6P09_00145). In general terms, the HM26-OE*sirR* overexpression strain displayed the lower expression levels of this gene in iron-limited cultures, while the deletion mutant exhibited heightened activation (Fig. 5). These results are consistent with SirR acting as a negative regulator of the expression of the gene encoding the metal binding protein under these conditions. Further analysis of the data from the control strain indicates that the expression of the transporter is influenced not only by SirR levels but also by the availability of iron.

Compared to the substrate-binding protein, the gene encoding the permease subunit of the iron-ABC transporter (E6P09_02480) appears to be regulated differently. Several explanations could account for this difference. One possibility is that iron homeostasis changes over time, leading to the permease being expressed either before or after the RNA samples were collected (Pi and Helmann 2017). Since the promoter regions of the genes analysed by qRT-PCR differ in the number of motif repetitions, a delayed or postponed regulation could be involved. Alternatively, the gene encoding the permease may be subject to additional regulatory mechanisms that differ from those controlling the metal binding protein. The differences observed between the two genes therefore suggest that regulation of iron uptake in *Hfx. mediterranei* cannot be explained solely by the action of a single transcriptional regulator(Martinez Pastor et al. 2023).

Interestingly, no significant differences in *sirR* expression levels were observed across different conditions, highlighting the pivotal role of iron supplementation or limitation in modulating transporter expression. Additionally, the results demonstrate that SirR exerts its regulatory function under both oxic and anoxic conditions (Fig. 5).

An additional aspect that also deserves further investigation is the apparent temporal dependence of the gene expression of both genes. In contrast to the early-growth RNA-Seq dataset, in which both genes were downregulated under denitrifying conditions (Miralles-Robledillo et al. 2024), qRT-PCR analyses and metal accumulation determinations were performed at the end of exponential growth (Miralles-Robledillo et al. 2024). Accordingly, we hypothesize that the expression of both genes involved in iron transport, as well as the expression of *sirR*, may vary over time during denitrification to maintain the metal homeostasis, as evidenced by disparities between data from RNAseq and RT-qPCR regarding the gene encoding the ABC transporter iron-binding like protein (Pi and Helmann 2017).

To investigate the potential molecular basis of SirR-mediated regulation, promoter regions of iron-related genes that were repressed during early denitrification were analysed for candidate regulatory sequences (Fig. 6). The consensus sequence identified using MEME software and manual inspection was selected not only based on this criterion, but also because of its high similarity to previously identified sequences associated with DtxR regulators in the *Archaea* domain (Leyn and Rodionov 2015; Martinez Pastor et al. 2023). Specifically, the motifs have been previously described in microorganisms of the order *Halobacteriale*s (Leyn and Rodionov 2015; Martinez Pastor et al. 2023).

To complement these findings with biochemical analyses, the purification of the SirR protein allowed the identification of this regulator as a homodimer (Fig. 7), which is consistent with what was observed in structural studies carried out with members of the DtxR family of transcriptional regulators (Pohl et al. 1998).

After the purification of SirR, Electrophoretic Mobility Shift Assays (EMSA) were conducted following a protocol adapted for halophilic proteins on agarose and on polyacrylamide gels (Matarredona et al., 2024) using the purified SirR protein. Despite multiple optimization attempts, these assays yielded negative results for SirR binding to the promoter regions of the genes encoding iron transporters listed in Supplementary Table 2 (Data not shown; details of the EMSA protocol followed were included in supplementary material)

Several explanations may account for the absence of detectable binding. First, electrophoretic assays involving halophilic proteins are technically challenging because these proteins require high salt concentrations to remain in their native structure. High ionic strength alters buffer conductivity and can interfere with sample migration, resolution and temperature control during electrophoresis (Gaudreault et al. 2009). Therefore, failure to detect a mobility shift does not necessarily exclude DNA binding under physiological conditions. In addition, if SirR activity depends on a specific metal or other ligand, the absence or suboptimal concentration of such a cofactor under the *in vitro* conditions used could prevent the formation of a stable SirR-DNA complex. Although different concentrations of iron and manganese were tested in the binding assays, the possibility that the conditions required for optimal metal-dependent DNA binding were not fully reproduced cannot be excluded.

An alternative explanation is that SirR does not bind directly to the promoter regions of these genes, suggesting its regulatory effects might be mediated through indirect mechanisms. Deletion of the *sirR* gene did not display drastic effects on growth or metal accumulation, despite the transcriptional changes observed for the candidate iron transport gene. These observations suggest that additional regulatory mechanisms may compensate for the loss of SirR and could contribute to the control of metal homeostasis in *Hfx. mediterranei*. Other DtxR regulators encoded in *Hfx. mediterranei* could also contribute to this response as part of a broader regulatory network, as has been shown in other haloarchaea (Martinez-Pastor et al. 2017; Martinez Pastor et al. 2023; Miralles-Robledillo et al. 2024). Further studies will therefore be required to fully elucidate the regulatory mechanisms underlying this response.

Figure 8 summarizes and integrates the key findings of this study, highlighting the metabolic and transcriptomic changes in *Hfx. mediterranei.* During early growth, the integration of RNA-Seq and ICP-MS data (Fig. 8, left panel), indicated that intracellular metals accumulate preferentially under oxic conditions, while the transition to denitrification is accompanied by decreased expression of several metal transport genes and increased *sirR* expression. At later stages of growth, qRT-PCR results and ICP-MS measurements (Fig. 8, right panel), indicated that the differences become less pronounced, and a distinct regulatory state appears to be established in which both sirR and transporter genes are

expressed at comparatively moderate levels. Under anoxic conditions, increased expression of some transport components coincides with higher intracellular metal accumulation. Together, these observations support a model in which metal homeostasis is dynamically adjusted according to both oxygen availability and growth phase rather than being governed by a single fixed regulatory response.

The accumulation of more metals in *Hfx. mediterranei* cells under denitrifying conditions in the stationary phase remains unclear. Based in the known mechanisms of denitrification, it can be deduced that due to the nature of the for key enzymes that catalyse the reduction (they are metalloenzymes) from nitrate to dinitrogen, the cell may need a pull of metals under these conditions. Similar behaviour has been observed in other microorganisms, which show higher accumulation and tolerance to heavy metals under microaerophilic/anaerobic conditions (Masaki et al. 2015; Jasso-Chávez et al. 2021; Upadhyay et al. 2023). The reasons for this phenomenon are attributed to lower levels of reactive oxygen species and less oxidative damage produced under this condition, which allowed the cells to better cope with the damage produced by high metal concentration, maintaining the metal homeostasis (Jasso-Chávez et al. 2021).

Alternatively, it is possible that *Hfx. mediterranei* may couple Fe^{2+} or Mn^{2+} oxidation with nitrate reduction under anoxic conditions, as seen in autotrophic/mixotrophic denitrification. (Zhang et al. 2015; Li et al. 2018; Xu et al. 2021; Gao et al. 2025; Wang et al. 2025). There is currently no experimental data available on this subject in the literature, so a clear answer cannot be currently provided. Therefore, the use of metals as electron donors for denitrification by *Hfx. mediterranei* is a worthwhile field, considering the possible applications.

From a biotechnological perspective the increased accumulation of metals under anoxic conditions is promising as a potential biotechnological tool and deserves further study, especially in the field of bioremediation (Voica et al. 2016). While previous studies have highlighted the potential of *Hfx. mediterranei* as bioremediation agents in wastewater treatment plants for the removal of nitrates, nitrites, and (per)chlorates from saline residues through denitrification, recent research also suggests that these microorganisms can reduce the concentration of certain metals in residues by intracellular accumulation (Martinez-Espinosa and Bonete 2007; Llorca and Martínez-Espinosa 2022; Saez-Zamacona et al. 2023). Given the heightened metal accumulation shown in this investigation when *Hfx. mediterranei* is cultivated under denitrifying conditions, there is the intriguing possibility of a dual bioremediation process with the same microorganism, simultaneously addressing nitrogen and chlorine species along with metal reduction.

This study sheds new light on how *Hfx. mediterranei* coordinates metal homeostasis under denitrifying conditions, revealing the regulatory role of the transcriptional repressor SirR in this process. Physiological, transcriptional, and biochemical analyses indicate that SirR acts as a metal-dependent regulator, influencing the intracellular accumulation of several transition metals, particularly iron, manganese, copper, zinc, and molybdenum, under both oxic and anoxic conditions.

Finally, this work improves our understanding of metal homeostasis in Hfx. mediterranei by highlighting the adaptive interplay between metal regulation and denitrification. Future research should aim to delineate the interactions between SirR, different DtxR family members and denitrification to fully reconstruct the regulatory network underlying metal homeostasis in this archaeon *Hfx. mediterranei*.

Declarations

Competing interests

The authors declare no competing interests.

Ethical Approval

Not applicable

Availability of data and materials

The data that supports the findings of this study are available in the supplementary material of this article.

Author contributions

Author contributions: JMM-R.: Conceptualization; data curation; formal analysis; investigation; methodology; visualization; writing—original draft. AGS.: Investigation. SR.: Conceptualization; methodology; resources; supervision; writing—review & editing. RMM-E.: Conceptualization; funding acquisition; project administration; resources; supervision; writing—review & editing. CP.: Conceptualization; funding acquisition; methodology; project administration; resources; supervision; writing—original draft; writing—review & editing.

Funding

This work was funded by Generalitat Valenciana, Spain (PROMETEO/2021/055), and VIGROB-309 (University of Alicante).

JMM-R was financed by the Banco Santander-University of Alicante grants for research stays abroad to carry out part of the experiments at the Sapienza University of Rome.

Acknowledgements

The authors of the manuscript would like to thank María Jose Nueda (University of Alicante) for her support with the statistical analysis.

References

1. Allers T, Ngo HP, Mevarech M, Lloyd RG (2004) Development of Additional Selectable Markers for the Halophilic Archaeon *Haloferax volcanii* Based on the *leuB* and *trpA* Genes. Appl Environ Microbiol 70. https://doi.org/10.1128/AEM.70.2.943-953.2004
2. Bailey TL, Johnson J, Grant CE, Noble WS (2015) The MEME Suite. Nucleic Acids Res. https://doi.org/10.1093/nar/gkv416
3. Bakken LR, Bergaust L, Liu B, Frostegård Å (2012) Regulation of denitrification at the cellular level: A clue to the understanding of N_2O emissions from soils. Philos Trans R Soc B Biol Sci 367:1226–1234. https://doi.org/10.1098/rstb.2011.0321
4. Bergaust L, van Spanning RJM, Frostegård Å, Bakken LR (2012) Expression of nitrous oxide reductase in *Paracoccus denitrificans* is regulated by oxygen and nitric oxide through FnrP and NNR. Microbiology 158:826–834. https://doi.org/10.1099/mic.0.054148-0
5. Bonete M-J, Pire C, Llorca FI, Camacho ML (1996) Glucose dehydrogenase from the halophilic Archaeon *Haloferax mediterranei* : Enzyme purification, characterisation and N-terminal sequence. FEBS Lett 383:227–229. https://doi.org/10.1016/0014-5793(96)00235-9
6. Crooks GE, Hon G, Chandonia JM, Brenner SE (2004) WebLogo: A sequence logo generator. Genome Res 14. https://doi.org/10.1101/gr.849004
7. Dyall-Smith ML (2008) Halohandbook
8. Erisman JW, Sutton MA, Galloway J, Klimont Z, Winiwarter W (2008) How a century of ammonia synthesis changed the world. Nat Geosci 1. https://doi.org/10.1038/ngeo325
9. Feng L, Yu Q, Li X, Ning X, Wang J, Zou J, Zhang L, Wang S, Hu J, Hu X, Bao Z (2013) Identification of Reference Genes for qRT-PCR Analysis in Yesso Scallop *Patinopecten yessoensis*. PLoS ONE 8. https://doi.org/10.1371/journal.pone.0075609
10. Galloway JN, Townsend AR, Erisman JW, Bekunda M, Cai Z, Freney JR, Martinelli LA, Seitzinger SP, Sutton MA (2008) Transformation of the nitrogen cycle: Recent trends, questions, and potential solutions. Science 320. https://doi.org/10.1126/science.1136674
11. Gao T, Li Y, Dai K, Meng F (2025) Electric syntrophy-driven modulation of Fe^0-dependent microbial denitrification. Water Res 268:122722. https://doi.org/10.1016/j.watres.2024.122722
12. Gaudreault M, Gingras ME, Lessard M, Leclerc S, Guérin SL (2009) Electrophoretic mobility shift assays for the analysis of DNA-protein interactions. Methods Mol Biol 543. https://doi.org/10.1007/978-1-60327-015-1_2
13. Golynskiy MV, Gunderson WA, Hendrich MP, Cohen SM (2006) Metal Binding Studies and EPR Spectroscopy of the Manganese Transport Regulator MntR. Biochemistry 45:15359–15372. https://doi.org/10.1021/bi0607406
14. Granger JB, Lu Z, Ferguson JB, Santa Maria PJ, Novak WRP (2013) Cloning, expression, purification and characterization of an iron-dependent regulator protein from *Thermobifida fusca*. Protein Expr Purif 92:190–194. https://doi.org/10.1016/j.pep.2013.09.010

15. Haque RU, Paradisi F, Allers T (2020) *Haloferax volcanii* for biotechnology applications: challenges, current state and perspectives. Appl Microbiol Biotechnol 104:1371. https://doi.org/10.1007/S00253-019-10314-2
16. Haque RU, Paradisi F, Allers T (2019) *Haloferax volcanii* as immobilised whole cell biocatalyst: new applications for halophilic systems. Appl Microbiol Biotechnol. https://doi.org/10.1007/S00253-019-09725-Y
17. Iuchi S, Weiner L (1996) Cellular and molecular physiology of *Escherichia coli* in the adaptation to aerobic environments. J Biochem (Tokyo) 120:1055–1063. https://doi.org/10.1093/oxfordjournals.jbchem.a021519
18. Jasso-Chávez R, Campos-García ML, Vega-Segura A, Pichardo-Ramos G, Silva-Flores M, Santiago-Martínez MG, Feregrino-Mondragón RD, Sánchez-Thomas R, García-Contreras R, Torres-Márquez ME, Moreno-Sánchez R (2021) Microaerophilia enhances heavy metal biosorption and internal binding by polyphosphates in photosynthetic *Euglena gracilis*. Algal Res 58. https://doi.org/10.1016/j.algal.2021.102384
19. Kuypers MMM, Marchant HK, Kartal B (2018) The microbial nitrogen-cycling network. Nat Rev Microbiol 16:263–276. https://doi.org/10.1038/NRMICRO.2018.9
20. Leyn SA, Rodionov DA (2015) Comparative genomics of DtxR family regulons for metal homeostasis in *Archaea*. J Bacteriol 197:451–458. https://doi.org/10.1128/JB.02386-14/SUPPL_FILE/ZJB999093458SO1.PDF
21. Li S, Li X, Li F (2018) Fe(II) oxidation and nitrate reduction by a denitrifying bacterium, *Pseudomonas stutzeri* LS-2, isolated from paddy soil. J Soils Sediments 18:1668–1678. https://doi.org/10.1007/s11368-017-1883-1
22. Lledó B, Martínez-Espinosa RM, Marhuenda-Egea FC, Bonete MJ (2004) Respiratory nitrate reductase from haloarchaeon *Haloferax mediterranei*: biochemical and genetic analysis. Biochim Biophys Acta BBA - Gen Subj 1674:50–59. https://doi.org/10.1016/j.bbagen.2004.05.007
23. Llorca MG, Martínez-Espinosa RM (2022) Assessment of *Haloferax mediterranei* Genome in Search of Copper-Molecular Machinery With Potential Applications for Bioremediation. Front Microbiol 13. https://doi.org/10.3389/FMICB.2022.895296
24. Locher KP, Lee AT, Rees DC (2002) The *E. coli* BtuCD structure: A framework for ABC transporter architecture and mechanism. Science 296. https://doi.org/10.1126/science.1071142
25. Ma Z, Jacobson FE, Giedroc DP (2009) Metal Transporters and Metal Sensors: How Coordination Chemistry Controls Bacterial Metal Homeostasis. October 109
26. Martin JE, Waters LS, Storz G, Imlay JA (2015) The *Escherichia coli* Small Protein MntS and Exporter MntP Optimize the Intracellular Concentration of Manganese. PLoS Genet 11. https://doi.org/10.1371/journal.pgen.1004977
27. Martinez-Espinosa RM, Bonete MJ (2007) Bioremediation of chlorate and perchlorate salted water using *Haloferax mediterranei*. J Biotechnol 131. https://doi.org/10.1016/j.jbiotec.2007.07.411

28. Martinez-Pastor M, Lancaster WA, Tonner PD, Adams MWW, Schmid AK (2017) A transcription network of interlocking positive feedback loops maintains intracellular iron balance in *archaea*. Nucleic Acids Res 45:9990–10001. https://doi.org/10.1093/NAR/GKX662
29. Martinez Pastor M, Sakrikar S, Hwang S, Hackley RK, Soborowski AL, Maupin-Furlow JA, Schmid AK (2023) TroR is the primary regulator of the iron homeostasis transcription network in the halophilic archaeon *Haloferax volcanii*. Nucleic Acids Res gkad997. https://doi.org/10.1093/nar/gkad997
30. Masaki Y, Hirajima T, Sasaki K, Okibe N (2015) Bioreduction and immobilization of hexavalent chromium by the extremely acidophilic Fe(III)-reducing bacterium *Acidocella aromatica* strain PFBC. https://doi.org/10.1007/s00792-015-0733-6. Extremophiles 19
31. Miralles-Robledillo JM, Martínez-Espinosa RM, Pire C (2024) Transcriptomic profiling of haloarchaeal denitrification through RNA-Seq analysis. Appl Environ Microbiol 90:e00571–e00524. https://doi.org/10.1128/aem.00571-24
32. Miralles-Robledillo JM, Martínez-Espinosa RM, Pire C (2023) Analysis of the external signals driving the transcriptional regulation of the main genes involved in denitrification in *Haloferax mediterranei*. Front Microbiol 14:676. https://doi.org/10.3389/FMICB.2023.1109550
33. Olaya-Abril A, Luque-Almagro VM, Hidalgo-Carrillo J, Chicano-Gálvez E, Urbano FJ, Moreno-Vivián C, Richardson DJ, Roldán MD (2022) The NtrYX Two-Component System of *Paracoccus denitrificans* Is Required for the Maintenance of Cellular Iron Homeostasis and for a Complete Denitrification under Iron-Limited Conditions. Int J Mol Sci 23:9172. https://doi.org/10.3390/ijms23169172
34. Parveen S, Bishai WR, Murphy JR (2019) *Corynebacterium diphtheriae*: Diphtheria Toxin, the *tox* Operon, and Its Regulation by Fe^{2+} Activation of apo-DtxR. Microbiol Spectr 7. https://doi.org/10.1128/MICROBIOLSPEC.GPP3-0063-2019
35. Pedro-Roig L, Lange C, Bonete MJ, Soppa J, Maupin-Furlow J (2013) Nitrogen regulation of protein-protein interactions and transcript levels of GlnK PII regulator and AmtB ammonium transporter homologs in *Archaea*. MicrobiologyOpen 2:826–840. https://doi.org/10.1002/MBO3.120
36. Pi H, Helmann JD (2017) Sequential induction of Fur-regulated genes in response to iron limitation in *Bacillus subtilis*. Proc Natl Acad Sci 114:12785–12790. https://doi.org/10.1073/pnas.1713008114
37. Pohl E, Holmes RK, Hol WGJ (1998) Motion of the DNA-binding domain with respect to the core of the diphtheria toxin repressor (DtxR) revealed in the crystal structures of apo- and holo-DtxR. J Biol Chem 273. https://doi.org/10.1074/jbc.273.35.22420
38. Rodriguez-Valera F, Juez G, Kushner DJ (1983) *Halobacterium mediterranei* spec, nov., a New Carbohydrate-Utilizing Extreme Halophile. Syst Appl Microbiol 4:369–381. https://doi.org/10.1016/S0723-2020(83)80021-6
39. Rolfe MD, Rice CJ, Lucchini S, Pin C, Thompson A, Cameron ADS, Alston M, Stringer MF, Betts RP, Baranyi J, Peck MW, Hinton JCD (2012) Lag Phase Is a Distinct Growth Phase That Prepares *Bacteria* for Exponential Growth and Involves Transient Metal Accumulation. J Bacteriol 194:686–701. https://doi.org/10.1128/jb.06112-11

40. Saez-Zamacona I, Grindlay G, Martínez-Espinosa RM (2023) Evaluation of *Haloferax mediterranei* Strain R4 Capabilities for Cadmium Removal from Brines. Mar Drugs 21. https://doi.org/10.3390/md21020072
41. Sayers EW, Bolton EE, Brister JR, Canese K, Chan J, Comeau DC, Farrell CM, Feldgarden M, Fine AM, Funk K, Hatcher E, Kannan S, Kelly C, Kim S, Klimke W, Landrum MJ, Lathrop S, Lu Z, Madden TL, Malheiro A, Marchler-Bauer A, Murphy TD, Phan L, Pujar S, Rangwala SH, Schneider VA, Tse T, Wang J, Ye J, Trawick BW, Pruitt KD, Sherry ST (2023) Database resources of the National Center for Biotechnology Information in 2023. Nucleic Acids Res 51. https://doi.org/10.1093/nar/gkac1032
42. Schalk IJ, Guillon L (2013) Fate of ferrisiderophores after import across bacterial outer membranes: different iron release strategies are observed in the cytoplasm or periplasm depending on the siderophore pathways. Amino Acids 44:1267–1277. https://doi.org/10.1007/s00726-013-1468-2
43. Schmid AK, Pan M, Sharma K, Baliga NS (2011) Two transcription factors are necessary for iron homeostasis in a salt-dwelling archaeon. Nucleic Acids Res 39:2519. https://doi.org/10.1093/NAR/GKQ1211
44. Schmitt MP (2002) Analysis of a DtxR-like metalloregulatory protein, MntR, from *Corynebacterium diphtheriae* that controls expression of an ABC metal transporter by an Mn^{2+}-dependent mechanism. J Bacteriol 184. https://doi.org/10.1128/JB.184.24.6882-6892.2002
45. Schneider TD, Stephens RM (1990) Sequence logos: A new way to display consensus sequences. Nucleic Acids Res 18. https://doi.org/10.1093/nar/18.20.6097
46. Stocker TF, Qin D, Plattner G-K, Tignor M, Allen SK, Boschung J, Nauels A, Xia Y, Bex V, Midgley PM (2013) IPCC, 2013: Climate Change 2013: The Physical Science Basis. Contribution of Working Group I to the Fifth Assessment Report of the Intergovernmental Panel on Climate Change. IPCC AR5
47. Tao X, Murphy JR (1992) Binding of the metalloregulatory protein DtxR to the diphtheria *tox* operator requires a divalent heavy metal ion and protects the palindromic sequence from DNase I digestion. J Biol Chem 267. https://doi.org/10.1016/s0021-9258(19)36677-3
48. Tao X, Schiering N, Zeng H, -y, Ringe D, Murphy JR (1994) Iron, DtxR, and the regulation of diphtheria toxin expression. Mol Microbiol 14:191–197. https://doi.org/10.1111/J.1365-2958.1994.TB01280.X
49. Taylor SC, Nadeau K, Abbasi M, Lachance C, Nguyen M, Fenrich J (2019) The Ultimate qPCR Experiment: Producing Publication Quality, Reproducible Data the First Time. Trends Biotechnol 37. https://doi.org/10.1016/j.tibtech.2018.12.002
50. Torregrosa-Crespo J, Martínez-Espinosa RM, Esclapez J, Bautista V, Pire C, Camacho M, Richardson DJ, Bonete MJ (2016) Anaerobic Metabolism in *Haloferax* Genus: Denitrification as Case of Study. In: Advances in microbial physiology. pp 41–85
51. Torregrosa-Crespo J, Pire C, Bergaust L, Martínez-espinosa RM (2020a) *Haloferax mediterranei*, an Archaeal Model for Denitrification in Saline Systems, Characterized Through Integrated Physiological and Transcriptional Analyses. Front Microbiol 11:1–13. https://doi.org/10.3389/fmicb.2020.00768

52. Torregrosa-Crespo J, Pire C, Martínez-Espinosa RM, Bergaust L (2019) Denitrifying haloarchaea within the genus *Haloferax* display divergent respiratory phenotypes, with implications for their release of nitrogenous gases. Environ Microbiol 21:427–436. https://doi.org/10.1111/1462-2920.14474
53. Torregrosa-Crespo J, Pire C, Richardson DJ, Martínez-Espinosa RM (2020b) Exploring the Molecular Machinery of Denitrification in *Haloferax mediterranei* Through Proteomics. Front Microbiol 11:605859. https://doi.org/10.3389/fmicb.2020.605859
54. Upadhyay SK, Rani N, Kumar V, Mythili R, Jain D (2023) A review on simultaneous heavy metal removal and organo-contaminants degradation by potential microbes: Current findings and future outlook. Microbiol Res 273. https://doi.org/10.1016/j.micres.2023.127419
55. Voica DM, Bartha L, Banciu HL, Oren A (2016) Heavy metal resistance in halophilic *Bacteria* and *Archaea*. FEMS Microbiol Lett 363:fnw146. https://doi.org/10.1093/femsle/fnw146
56. Wang H, Chen N, Feng C, Deng Y (2021) Insights into heterotrophic denitrification diversity in wastewater treatment systems: Progress and future prospects based on different carbon sources. Sci Total Environ 780. https://doi.org/10.1016/j.scitotenv.2021.146521
57. Wang X, Li W, Yang S, He Z, Li Y, Wang Y, Li J (2025) Iron-dependent autotrophic denitrification as a novel microbial driven and iron-mediated denitrification process: A critical review. Environ Res 273:120808. https://doi.org/10.1016/j.envres.2025.120808
58. Weltzien FA, Pasqualini C, Vernier P, Dufour S (2005) A quantitative real-time RT-PCR assay for European eel tyrosine hydroxylase. In: General and Comparative Endocrinology
59. Xu B, Shi L, Zhong H, Wang K (2021) Investigation of Fe(II) and Mn(II) involved anoxic denitrification in agricultural soils with high manganese and iron contents. J Soils Sediments 21:452–468. https://doi.org/10.1007/s11368-020-02776-z
60. Zerulla K, Chimileski S, Nather D, Gophna U, Papke RT, Soppa J (2014) DNA as a phosphate storage polymer and the alternative advantages of polyploidy for growth or survival. PLoS ONE 9. https://doi.org/10.1371/journal.pone.0094819
61. Zhang H, Wang H, Yang K, Chang Q, Sun Y, Tian J, Long C (2015) Autotrophic denitrification with anaerobic Fe^{2+} oxidation by a novel *Pseudomonas* sp. W1. Water Sci Technol 71:1081–1087. https://doi.org/10.2166/wst.2015.071

Figures

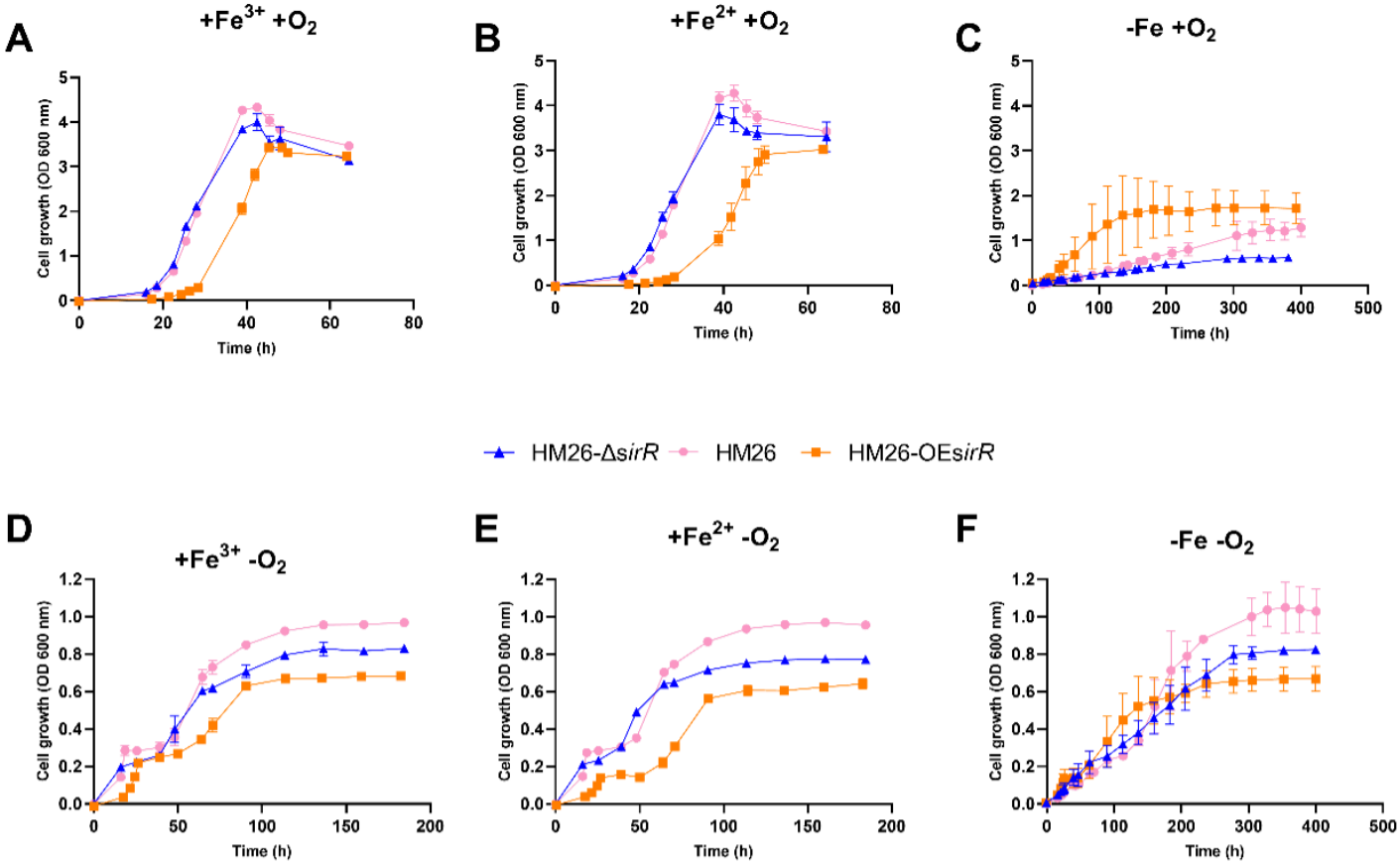


Figure 1

Growth curves of *Haloferax mediterranei* control (HM26 [Pink circles]) and modified strains (HM26-Δ*sirR* [Blue triangles] and HM26-OE*sirR* [Orange squares]) with or without iron supplementation and in the presence or absence of oxygen. **(a)** Aerobic cultures supplemented with $FeCl_3$; **(b)** Aerobic cultures supplemented with $FeCl_2{\cdot}4H_2O$; **(c)** Aerobic cultures without iron supplementation; **(d)** Anaerobic cultures supplemented with $FeCl_3$; **(e)** Anaerobic cultures supplemented with $FeCl_2{\cdot}4H_2O$; **(f)** Anaerobic cultures without iron supplementation.

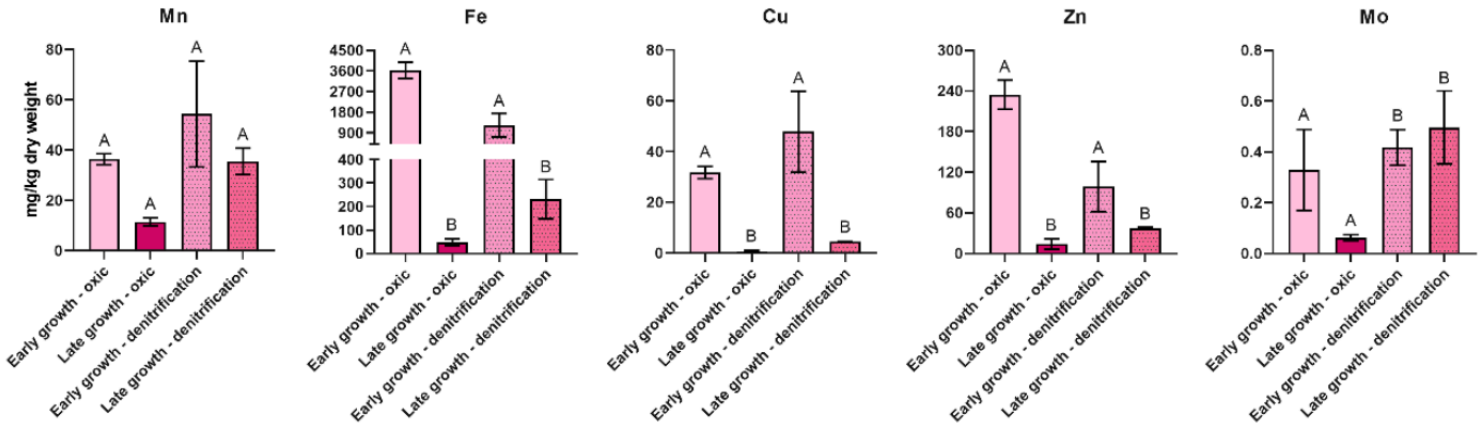


Figure 2

Intracellular accumulation of metals (iron, manganese, zinc, copper, and molybdenum) under different culture conditions in the control strain *Haloferax mediterranei* HM26 at different growth phases. Codes: Soft pink: Measurement taken at early growth stages; Dark pink: Measurement taken at late (stationary) growth stages; Dotted bars: Measurement taken under denitrifying conditions; Undotted bars: Measurement taken under oxic conditions. Different letters indicate statistically significant differences between growth phases or oxygen conditions from Kruskal–Wallis test.

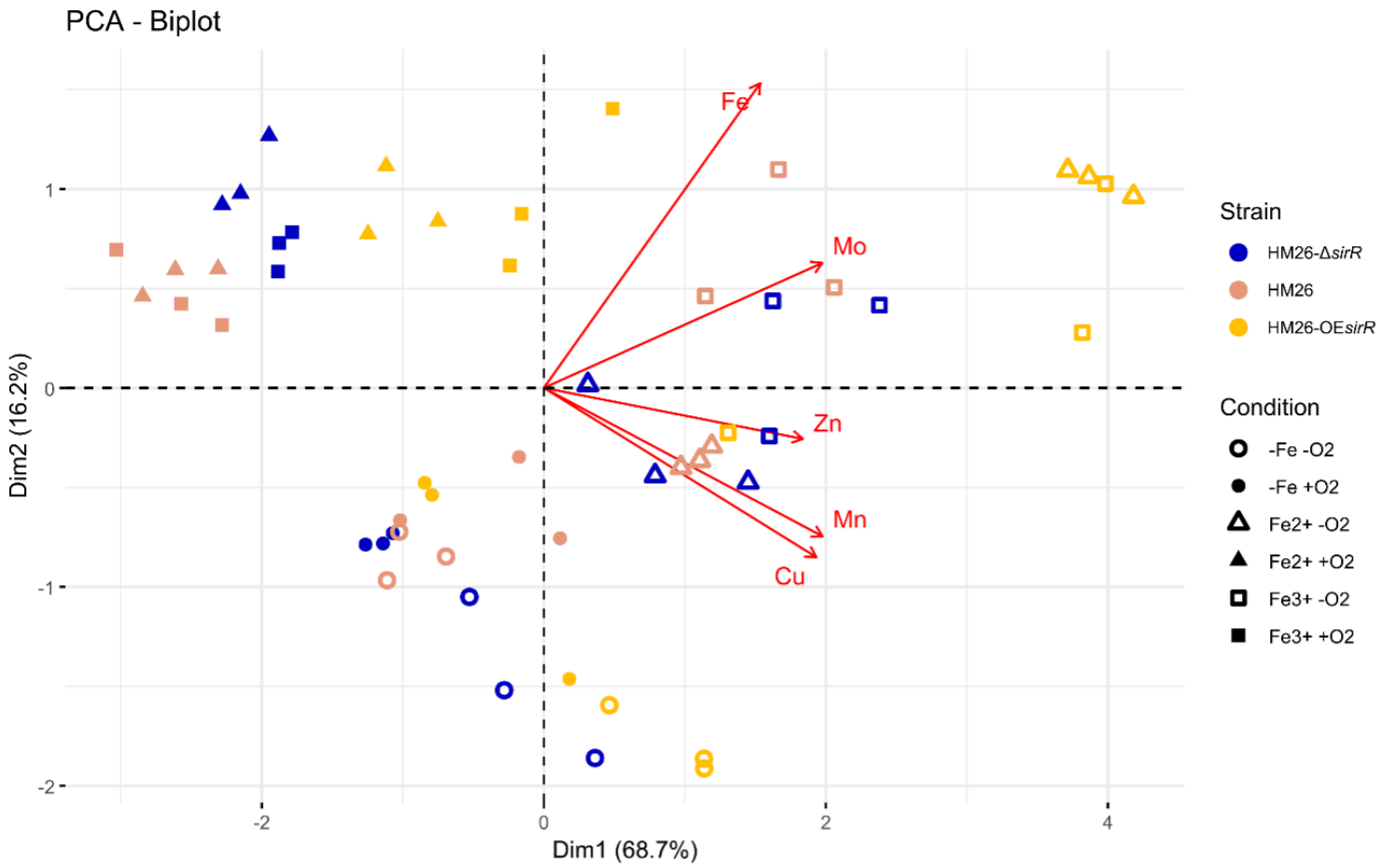


Figure 3

Principal component analysis of the study. Arrows indicate the contribution of the variables to the principal components of each dimension. In brackets is shown the percentage of explained variance for each dimension. Dim1: Dimension 1; Dim2: Dimension 2.

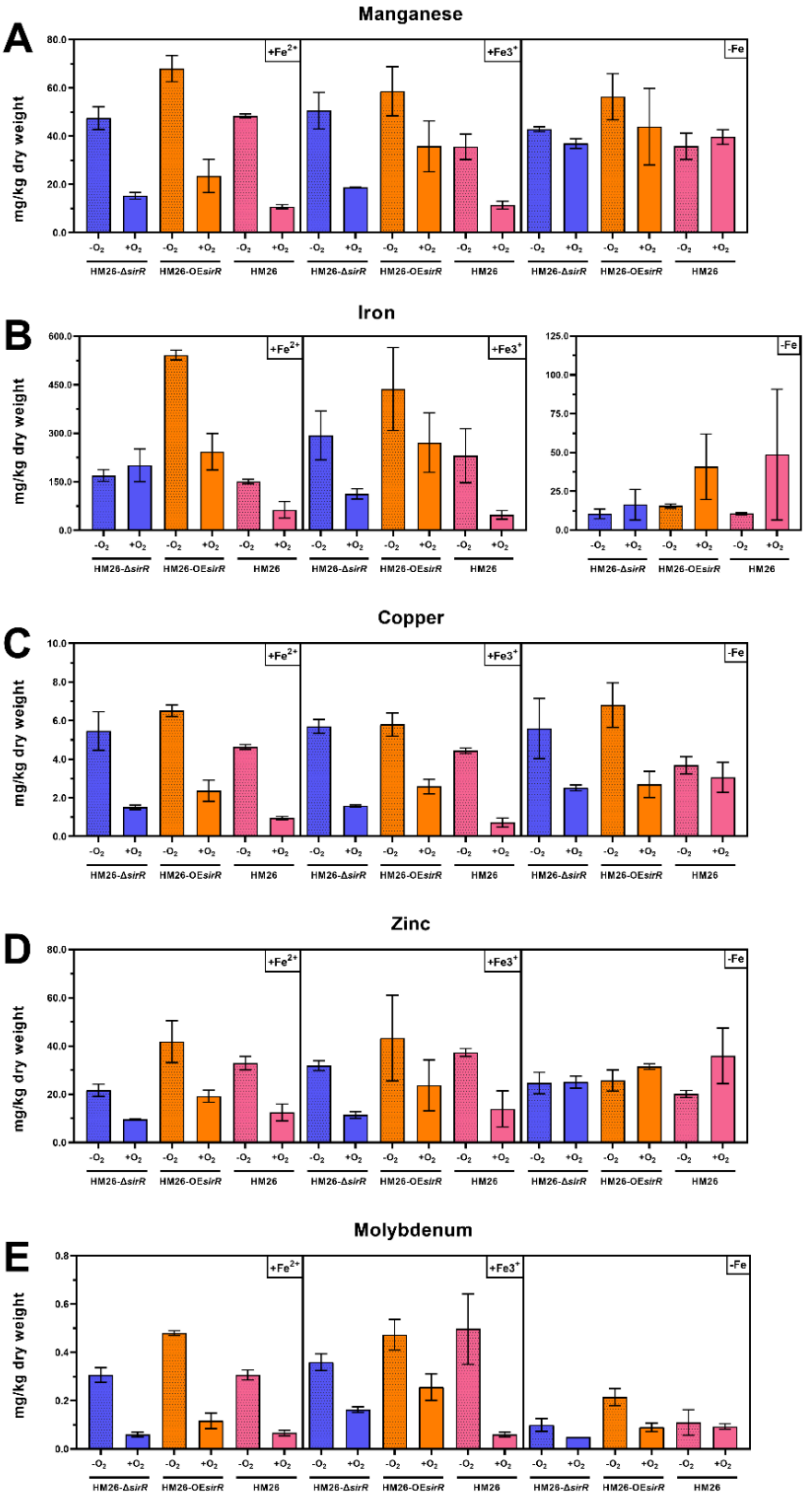


Figure 4

Intracellular accumulation of different metals in the three strains used in the study (pink: HM26; blue: HM26-Δ*sirR*; orange: HM26-OE*sirR*) under different culture conditions. Codes: $+Fe^{2+}$: cultures supplemented with ferrous iron; $+Fe^{3+}$: cultures supplemented with ferric iron; -Fe: cultures without iron supplementation; $+O_2$: oxic cultures; $-O_2$: anoxic cultures; Dotted bars: Measurements taken under

denitrifying conditions; Undotted bars: Measurement taken under oxic conditions. **(a)** Manganese **(b)** Iron **(c)** Copper **(d)** Zinc **(e)** Molybdenum.

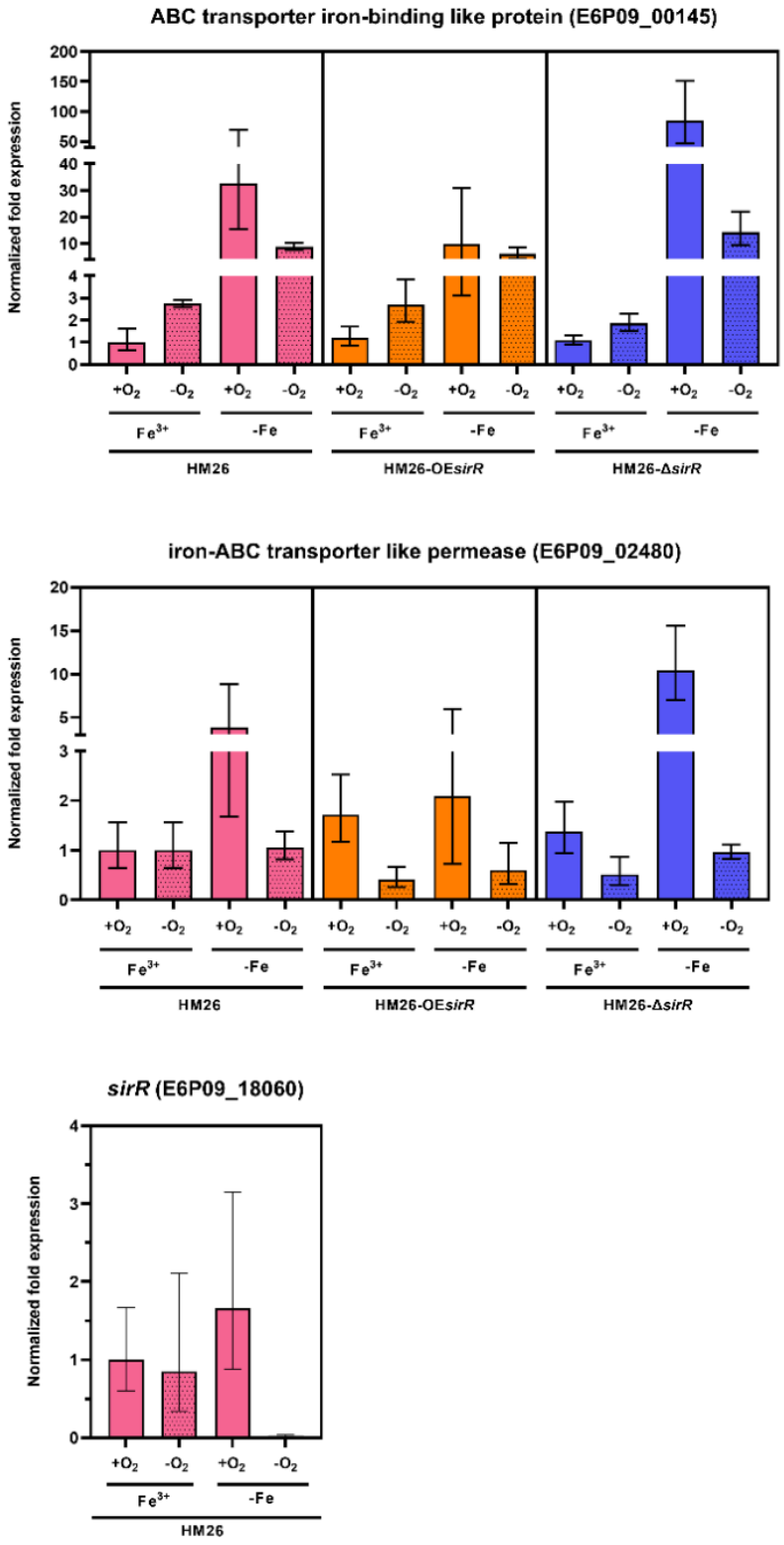


Figure 5

qRT-PCR results. Normalized fold expression of the genes E6P09_00145, E6P09_02480 and E6P09_18060 (NCBI Gene IDs), encoding for ABC transporter iron-binding like protein, iron-ABC

transporter like permease and *sirR,* respectively. 16s rRNA and cytochrome b genes were used as reference genes. The colours indicate the strain (pink: HM26; blue: HM26-Δ*sirR*; orange: HM26-OE*sirR*). Codes: $+Fe^{3+}$: cultures supplemented with ferric iron; -Fe: cultures without iron supplementation; $+O_2$: oxic cultures; $-O_2$: anoxic cultures; Dotted bars: Measurement taken under denitrifying conditions; Undotted bars: Measurement taken under oxic conditions.

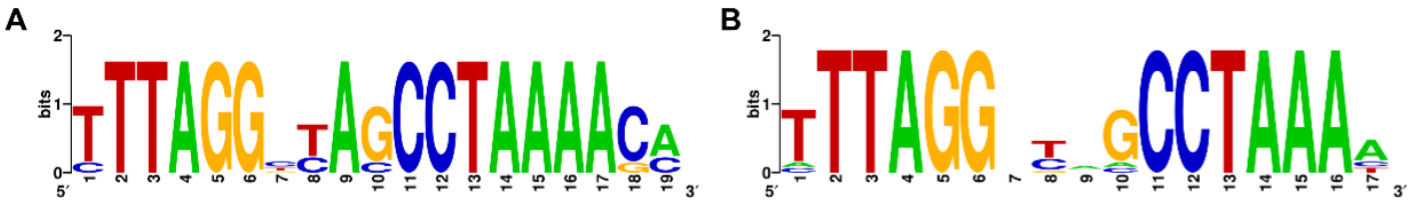


Figure 6

The consensus sequence found in the promoter region of iron-related genes showed a significant negative expression change under denitrifying conditions. **(a)** Motif found using MEME. **(b)** Motif found by manual search.

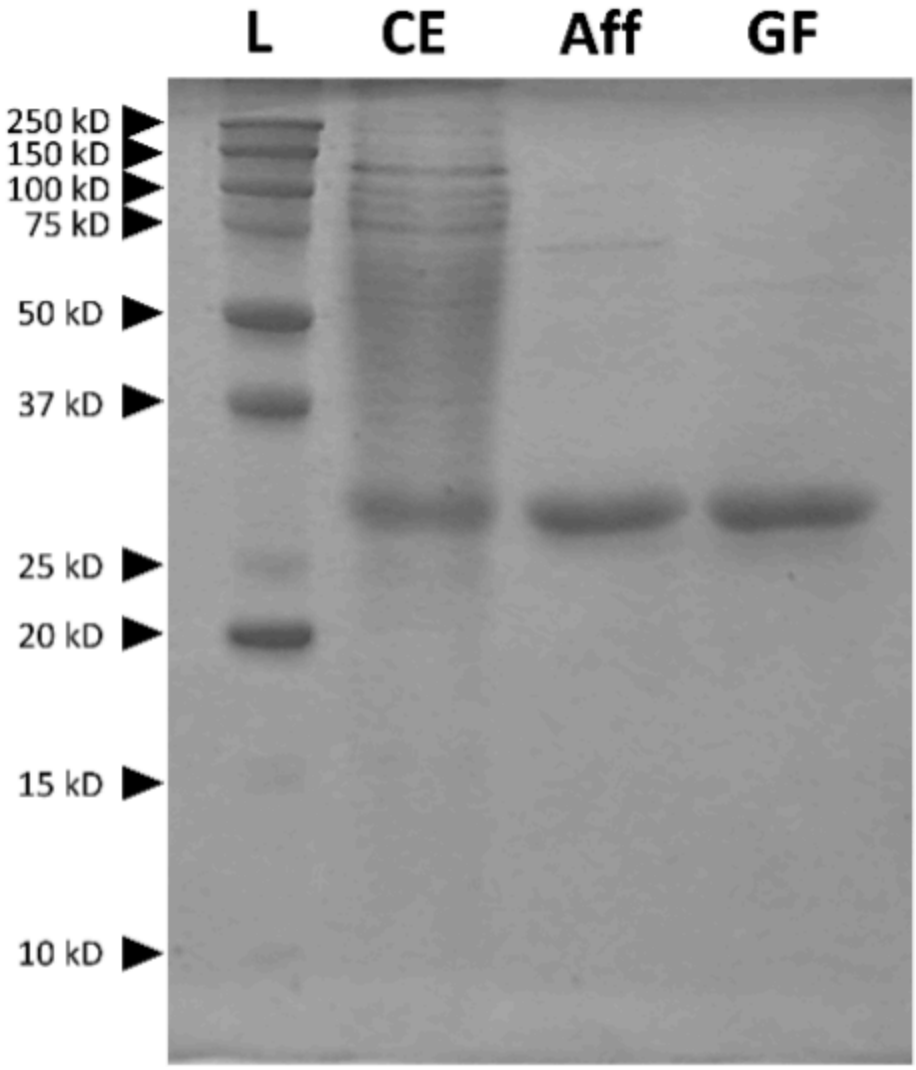


Figure 7

Purified His_6-SirR in 12% SDS-PAGE. L: Protein Ladder (Precision Plus Protein Dual Color Standards – BioRad); CE: Crude protein extract; Aff: His-tagged fraction from metal affinity chromatography; GF: HiPrep 16/60 Sephacryl S-100 HR fraction from gel filtration chromatography.

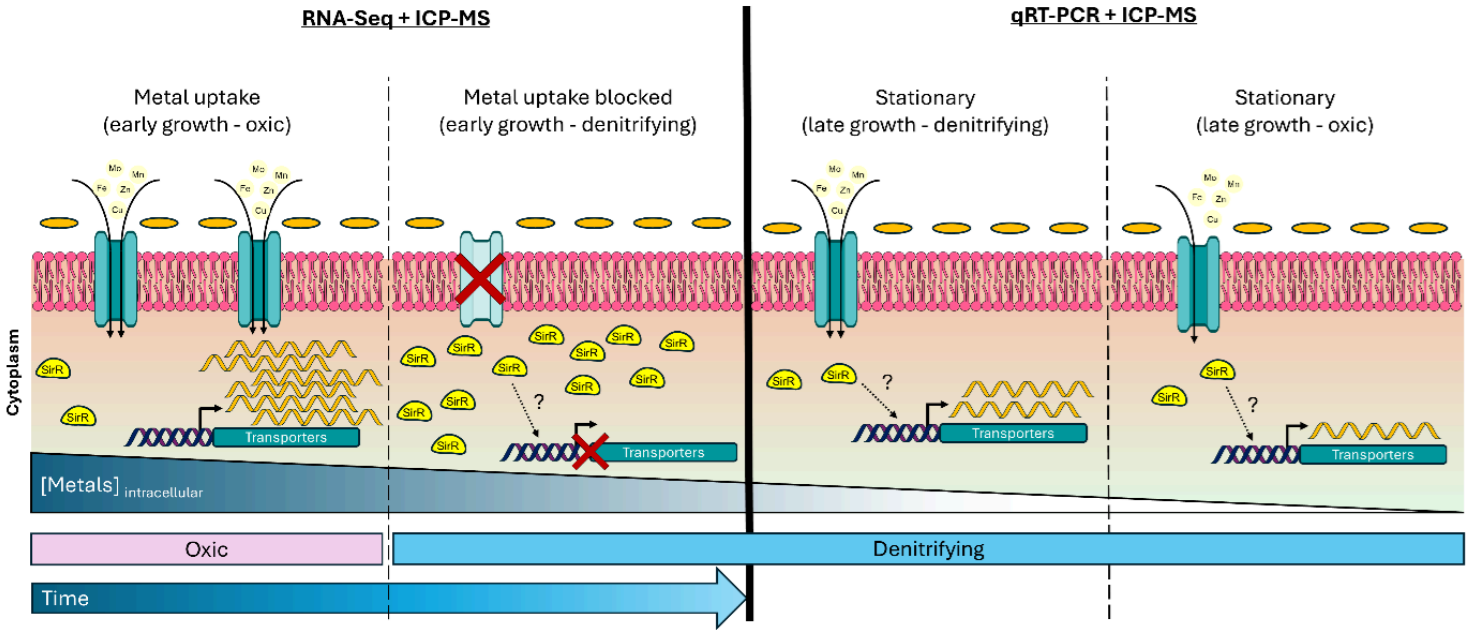


Figure 8

Summary of the key findings of this study. Metabolic changes and differences related to the intracellular metal accumulation and the expression levels of transporters and the transcriptional regulator SirR in *Haloferax mediterranei*. **Early Growth Stages (Left Panel):** Integration of RNA-Seq and ICP-MS data. **Stationary Phase (Right Panel):** Integration of qRT-PCR and ICP-MS data.

Supplementary Files

This is a list of supplementary files associated with this preprint. Click to download.

- Supplementarymaterial.docx